

Adaptive Robust Data-Driven Building Control via Bilevel Reformulation: An Experimental Result

Yingzhao Lian^{ID}, *Graduate Student Member, IEEE*, Jicheng Shi^{ID}, *Graduate Student Member, IEEE*, Manuel Koch^{ID}, and Colin Neil Jones^{ID}, *Senior Member, IEEE*

Abstract—Data-driven control approaches for the minimization of energy consumption of buildings have the potential to significantly reduce deployment costs and increase the uptake of advanced control in this sector. A number of recent approaches based on the application of Willems’ fundamental lemma for data-driven controller design from input/output measurements are very promising for deterministic linear time-invariant (LTI) systems. This article proposes a systematic way to handle unknown measurement noise and measurable process noise, and extends these data-driven control schemes to adaptive building control via a robust bilevel formulation, whose upper level ensures robustness and whose lower level guarantees prediction quality. Corresponding numerical improvements and an active excitation mechanism are proposed to enable a computationally efficient reliable operation. The efficacy of the proposed scheme is validated by a multizone building simulation and a real-world experiment on a single-zone conference building on the École Polytechnique Fédérale de Lausanne (EPFL) campus. The real-world experiment includes a 20-day nonstop test, where, without extra modeling effort, our proposed controller improves 18.4% energy efficiency against an industry-standard controller while also robustly ensuring occupant comfort.

Index Terms—Experimental building control, robust data-driven control.

I. INTRODUCTION

PREDICTIVE control techniques have recently been proven to be effective for controlling building heating, ventilation, and air conditioning (HVAC) systems with reduced energy consumption while simultaneously improving comfort. However, the cost of model building and commissioning has proven to be very high, and as a result, data-driven approaches for building energy saving have been receiving broad attention.

The motivation of this work is to develop a practical robust adaptive data-driven building controller, whose time-varying linear dynamics are disturbed by measurable process noise including outdoor temperature and solar radiation, and whose

Manuscript received 29 September 2022; revised 14 February 2023; accepted 15 March 2023. Date of publication 30 March 2023; date of current version 23 October 2023. This work was supported by the Swiss National Science Foundation through the RISK project (Risk Aware Data-Driven Demand Response) under Grant 200021 175627. (Yingzhao Lian and Jicheng Shi contributed equally to this work.) Recommended by Associate Editor T. Hatanaka. (Corresponding author: Colin Neil Jones.)

The authors are with the Automatic Control Laboratory, École Polytechnique Fédérale de Lausanne (EPFL), CH-1015 Lausanne, Switzerland (e-mail: yingzhao.lian@epfl.ch; jicheng.shi@epfl.ch; manuel.pascal.koch@epfl.ch; colin.jones@epfl.ch).

Color versions of one or more figures in this article are available at <https://doi.org/10.1109/TCST.2023.3259641>.

Digital Object Identifier 10.1109/TCST.2023.3259641

output measurements are contaminated by unknown measurement noise. Beyond building control, systems with measurable disturbances are ubiquitous, especially in energy-related applications: solar radiation in photovoltaic power systems, electricity demand in power grids, and power generation in airborne wind energy systems, to name a few. The main contributions of this article are summarized as follows.

- 1) Propose a novel trajectory prediction method, where a new upper bound of the Wasserstein distance between the trajectory determined by Willems’ fundamental lemma and the noisy measured sequence is minimized.
- 2) Propose a tractable robust bilevel data-driven building controller, whose lower level problem applies the trajectory prediction scheme proposed in the last point.
- 3) Propose a numerically efficient extension of the proposed bilevel scheme to linear time-varying (LTV) dynamics. This includes an active excitation scheme to maintain robust online data updates and numerical details for efficient online update of the matrix inversion used in the algorithm.
- 4) Experimental validation of the proposed scheme on a real-world building.

A. Previous Work

Data can be used to model building dynamics [14] or directly generate/improve control policies. Due to seasonal variations [4] and component wear, building dynamics are usually slowly time-varying, and adaptive model predictive control (MPC) has been introduced to combine online parameter estimation and control in [27]. For example, the experiment in [54] adaptively estimates the model of an evaporator in the HVAC system, which is then used to control the valve set-points. Maasoumy et al. [38] run an extended Kalman filter to achieve online parameter adaptation before the estimated model is used in an MPC controller. However, these parameter-estimation-based adaptive methods usually require a priori knowledge about the structure of the building dynamics and/or the HVAC systems.

Beyond running through a modeling/estimation procedure, data can be used to refine a control policy. The main approaches in this direction include reinforcement learning (RL) [52] and iterative learning control (ILC) [16]. In particular, ILC has been used for buildings with fixed heating/occupant schedules [43], [60] and RL for learning

a building control policy that is not necessarily iterative [17]. To run these learning schemes, a high-fidelity building simulator is usually required, and therefore, publications on successful experiments with HVAC systems are rare, with a few exceptions being [18], [44], [33], [63], and [48].

Beyond RL and ILC, data can also be used to directly characterize the system's responses from a behavioral theoretic viewpoint [57]. Willems' fundamental lemma is such a tool that provides a characterization of linear time-invariant (LTI) systems from measured input and output trajectories. Such a characterization offers a convenient interface to data-driven controller design [19], [22], [41], [42]. Motivated by the simplicity and effectiveness of the fundamental lemma, its extension to a more general setting is attracting broad attention, including nonlinear extensions [8], [13], [35], [47], data informativity [62], descriptor system [49], and so on [56].

Even for LTI systems, the absence of output measurement noise in the standard Willems' fundamental lemma limits its practicality. To accommodate this issue, a wide range of researchers are studying this challenge. In [10], [55], and [9], classic robust control design tools, such as linear fractional transforms, have been proposed to design robust linear feedback controllers. Parallel to the studies in linear feedback control laws, robustness in predictive control schemes has also been studied [21], [25], [59], where regularization is the main tool applied to deal with measurement noise. Coulson et al. [21] show that the regularization is related to the distributional robustness of the system uncertainty (including measurement noise). Dorfler et al. [25] study a different viewpoint, where the regularization is linked to the loss function used in the system identification. When convex relaxation is applied, the loss function in the system identification procedure results in a regularization term [25], [40].

Building on this regularization viewpoint, data-driven controllers based on Willems' fundamental lemma have been successfully deployed on different real-world systems, such as a quadrotor [28] and a four-tank system [11]. However, tuning the regularization weight still poses a nontrivial challenge, and an exhaustive search based on simulation is commonly used [40].

Motivated by the discussions above, this article proposes a novel bilevel data-driven predictive controller. Instead of solving the general case with unknown process/measurement noise, this article focuses on applications with unknown measurement noise and measurable process noise, such as building control (see Section II-B for more details). In the following, background knowledge is reviewed in Section II. In Section II-B, the problem setup is presented, and the proposed predictive controller is summarized in (5). Sections III and IV then accordingly develop and analyze the proposed scheme in the LTI and the LTV cases accordingly. Regarding the LTV systems, an active excitation mechanism is introduced in Section IV-A accompanied by numerical details of efficient online updates in Section IV-B. The complete robust adaptive data-driven controller is summarized in Algorithm 1. The effectiveness of the proposed algorithm is first validated through temperature control of a multizone building in Section V, followed by the experimental results

with an entire building on the EPFL campus in Section VI. A conclusion of this article is given in Section VII.

Notations: $\mathcal{N}(\mu, \Sigma)$ denotes a Gaussian distribution with mean μ and covariance Σ . \otimes is the symbol for the Kronecker product. \times is the symbol for the set product operation (i.e., $A \times B := \{(x, y) | x \in A, y \in B\}$), \oplus is the symbol of Minkowski sum (i.e., $A \oplus B := \{x | \exists x_1 \in A, x_2 \in B, x = x_1 + x_2\}$), and \ominus is the symbol of Pontryagin difference (i.e., $A \ominus B := \{x | x + y \in A, \forall y \in B\}$). $\text{colspan}(A)$ denotes the column space (i.e., range) of the matrix A . I_n is the $n \times n$ identity matrix, \mathbf{O} and $\mathbf{0}$ are the zero matrix and the zero vector, respectively. $\|\cdot\|$ denotes the Euclidean two-norm. $x := \{x_i\}_{i=1}^T$ denotes a sequence of size T indexed by i . x_i denotes the measurement of x at time i , and $x_{1:L} := [x_1^\top, x_2^\top, \dots, x_L^\top]^\top$ denotes a concatenated sequence of x_i ranging from x_1 to x_L ; we drop the index to improve clarity if the intention is clear from the context.

II. PRELIMINARIES

Definition 1: A Hankel matrix of depth L associated with a vector-valued signal sequence $s := \{s_i\}_{i=1}^T$, $s_i \in \mathbb{R}^{n_s}$ is

$$\mathfrak{H}_L(s) := \begin{bmatrix} s_1 & s_2 & \dots & s_{T-L+1} \\ s_2 & s_3 & \dots & s_{T-L+2} \\ \vdots & \vdots & & \vdots \\ s_L & s_{L+1} & \dots & s_T \end{bmatrix}.$$

A deterministic LTI system, dubbed $\mathfrak{B}(A, B, C, D)$, is defined as

$$x_{i+1} = Ax_i + Bu_i, \quad y_i = Cx_i + Du_i \quad (1)$$

whose order is n_x . n_u and n_y denote its input and output dimensions, respectively. An L -step trajectory generated by this system is

$$[u_{1:L} \quad y_{1:L}] := [u_1^\top \quad \dots \quad u_L^\top \quad y_1^\top \quad \dots \quad y_L^\top]^\top.$$

The set of all possible L -step trajectories generated by $\mathfrak{B}(A, B, C, D)$ is denoted by $\mathfrak{B}_L(A, B, C, D)$.

For the sake of consistency, a datapoint coming from the historical dataset is marked by boldface subscript \mathbf{d} . Given a sequence of input-output measurements $\{u_{\mathbf{d},i}, y_{\mathbf{d},i}\}_{i=1}^T$, we call the input sequence persistently exciting of order L if $\mathfrak{H}_L(u_{\mathbf{d}})$ is full row rank. By building the following n_c -column stacked Hankel matrix:

$$\mathfrak{H}_L(u_{\mathbf{d}}, y_{\mathbf{d}}) := \begin{bmatrix} \mathfrak{H}_L(u_{\mathbf{d}}) \\ \mathfrak{H}_L(y_{\mathbf{d}}) \end{bmatrix} \quad (2)$$

we state Willems' fundamental lemma as follows.

Lemma 1 ([58, Th. 1]): Consider a controllable linear system, and assume that $\{u_{\mathbf{d},i}\}_{i=1}^T$ is persistently exciting of order $L+n_x$. The condition $\text{colspan}(\mathfrak{H}_L(u_{\mathbf{d}}, y_{\mathbf{d}})) = \mathfrak{B}_L(A, B, C, D)$ holds.

For the sake of consistency, L is reserved for the length of the system responses, and n_c denotes the number of columns in a Hankel matrix.

A data-driven control scheme has been proposed in [19] and [41], where Lemma 1 generates a trajectory prediction. We

postpone the detailed discussion about the existing methods to Section III-C, in order to better articulate the idea behind the existing methods and to better compare the difference between the proposed and existing methods.

A. Wasserstein Distance

The 2-Wasserstein distance between two distributions \mathbb{P}_x and \mathbb{P}_y is defined by

$$W(\mathbb{P}_x, \mathbb{P}_y) := \left(\inf_{\gamma \in \Gamma(\mathbb{P}_x, \mathbb{P}_y)} \mathbb{E}_{(x,y) \sim \gamma} \|x - y\|^2 \right)^{\frac{1}{2}}$$

where $\Gamma(\mathbb{P}_x, \mathbb{P}_y)$ is the family of joint distributions whose marginals are \mathbb{P}_x and \mathbb{P}_y . The 2-Wasserstein distance models the optimal transport between \mathbb{P}_x and \mathbb{P}_y in terms of the Euclidean distance. If $\mathbb{P}_x \sim \mathcal{N}(\mu_x, \Sigma_x)$ and $\mathbb{P}_y \sim \mathcal{N}(\mu_y, \Sigma_y)$, then the squared 2-Wasserstein distance has a closed-form [26]

$$W(\mathbb{P}_x, \mathbb{P}_y)^2 = \|\mu_x - \mu_y\|^2 + \text{tr}(\Sigma_x + \Sigma_y - 2(\Sigma_x \Sigma_y)^{\frac{1}{2}}). \quad (3)$$

B. Setting the Stage

Recall the main properties in building applications.

- 1) The system dynamics are slowly time-varying.
- 2) The building dynamics evolve under strong measurable process noise, such as solar radiation and outdoor temperature.
- 3) Because of the activity of the occupants, the output measurements, particularly the measurements of the indoor temperature, are noisy.

Given these properties, this work focuses on the following uncertain LTV system:

$$\begin{aligned} x_{i+1} &= A_i x_i + B_i u_i + E_i w_i \\ \bar{y}_i &= C_i x_i + D_i u_i, \quad y_i = \bar{y}_i + v_i \end{aligned} \quad (4)$$

where $w_i \in \mathbb{R}^{n_w}$ is the bounded measurable process noise and $v_i \sim \mathcal{N}(0, \Sigma_v)$ with $v_i \in \mathbb{R}^{n_y}$ independent identically distributed (i.i.d.) unknown measurement noise. In particular, \bar{y} is the system output, which is unknown, and y is the measurement read out from the sensors. In particular, in the building control problem, w mostly reflects the external temperature, solar radiation, occupancy, and so on. Note that LTI systems are special cases of the LTV systems (4).

In a similar manner to [32] and [34], by viewing w as uncontrolled inputs, Lemma 1 can be generalized, and the corresponding L -step trajectory is augmented to

$$[u_{1:L} \ w_{1:L} \ y_{1:L}] := [u_1^\top \ \cdots \ u_L^\top \ w_1^\top \ \cdots \ w_L^\top \ y_1^\top \ \cdots \ y_L^\top]^\top.$$

Based on this idea, the rest of this article will develop and analyze the following bilevel predictive control problem step

by step:

$$\min_{\substack{y_{\text{pred}} \\ \bar{u}_{\text{pred}}, K}} J(y_{\text{pred}}, u_{\text{pred}}) \quad (5a)$$

$$\text{s.t. } \forall \tilde{w}_{\text{pred}} \in \bar{w} \oplus \tilde{\mathcal{W}} \quad (5b)$$

$$y_{\text{pred}} = \mathfrak{H}_{L,\text{pred}}(y_d)g \in \mathcal{Y} \quad (5c)$$

$$g \in \arg \min_{g_l, \sigma_l} \frac{1}{2} \|\sigma_l\|^2 + \frac{1}{2} g_l^\top \mathcal{E}_g g_l \quad (5d)$$

$$\text{s.t. } \begin{bmatrix} \mathfrak{H}_{L,\text{init}}(y_d) \\ \mathfrak{H}_{L,\text{init}}(u_d) \\ \mathfrak{H}_{L,\text{init}}(\tilde{w}_d) \\ \mathfrak{H}_{L,\text{pred}}(u_d) \\ \mathfrak{H}_{L,\text{pred}}(\tilde{w}_d) \end{bmatrix} g_l = \begin{bmatrix} y_{\text{init}} + \sigma_l \\ u_{\text{init}} \\ \tilde{w}_{\text{init}} \\ u_{\text{pred}} \\ \tilde{w}_{\text{pred}} \end{bmatrix} \quad (5e)$$

where $J(\cdot, \cdot)$ is a convex objective function, and $\tilde{\mathcal{U}}$ and \mathcal{Y} denote compact convex constraint sets on the input and the output. $\bar{w} \oplus \tilde{\mathcal{W}}$ models the set of possible future process noise with \bar{w} being the nominal future process noise and $\tilde{\mathcal{W}}$ being the quantified uncertainty. In addition, the tight input constraint is \mathcal{U} , and $\tilde{\mathcal{U}}$ is its tightening (i.e., $\tilde{\mathcal{U}} \subseteq \mathcal{U}$). $\tilde{\mathcal{W}}$ is an augmented set of actual process noise, and the set of the actual process noise is \mathcal{W} (i.e., $\exists n \geq 0$ such that $\tilde{\mathcal{W}} \subset \mathcal{W} \times \mathbb{R}^n$). The selection of both $\tilde{\mathcal{U}}$ and $\tilde{\mathcal{W}}$ will be elaborated in Section III-B. u_{init} , \tilde{w}_{init} , and y_{init} are t_{init} -step sequences of the measured inputs, process noise, and outputs preceding the current point in time. Accordingly, u_{pred} , \tilde{w}_{pred} , and y_{pred} are the corresponding n_h -step predictive sequences viewed from the current time step. The matrix $\mathfrak{H}_L(y_d)$ is split into two sub-Hankel matrices

$$\mathfrak{H}_L(y_d) = \begin{bmatrix} \mathfrak{H}_{L,\text{init}}(y_d) \\ \mathfrak{H}_{L,\text{pred}}(y_d) \end{bmatrix}.$$

The matrix $\mathfrak{H}_{L,\text{init}}(y_d)$ is of depth t_{init} , and the depth of $\mathfrak{H}_{L,\text{pred}}(y_d)$ is the prediction horizon n_h such that $t_{\text{init}} + n_h = L$. The matrices $\mathfrak{H}_{L,\text{init}}(u_d)$, $\mathfrak{H}_{L,\text{pred}}(u_d)$, $\mathfrak{H}_{L,\text{init}}(\tilde{w}_d)$, and $\mathfrak{H}_{L,\text{pred}}(\tilde{w}_d)$ are defined similarly. The choice of t_{init} is made to ensure a unique estimation of the initial state; please refer to [42] for more details. Furthermore, recall the condition of Willems' fundamental Lemma 1; the proposed scheme requires the following assumption:

Assumption 1: $\{u_d, \tilde{w}_d\}$ is persistently exciting of order $L + n_x$.

The proposed scheme (5) is bilevel, where the penalty weight \mathcal{E}_g , the set of disturbances $\tilde{\mathcal{W}}$, and the tightened input constraints $\tilde{\mathcal{U}}$ vary with respect to the working conditions. The selections of these terms will be elaborated on in Section IV. In Section III, a rigorous setup for LTI systems will first be developed to show the logic behind the bilevel formulation. The extension to the LTV system and the computational details will then be discussed in Section IV.

III. ROBUST BILEVEL DATA-DRIVEN CONTROL FOR LTI SYSTEMS

In this part, we will establish a rigorous mathematical framework for our proposed bilevel scheme (5) by considering

the LTI version of the targeted time-varying dynamics (4). The LTI dynamics satisfy

$$A_i = A_j, \quad B_i = B_j, \quad C_i = C_j, \quad D_i = D_j, \quad E_i = E_j \quad \forall i, j.$$

Note that the output trajectory prediction with respect to a given control input sequence u_{pred} is the key component for predictive control. In this section, we will show that this can be done by minimizing a Wasserstein distance upper bound between the trajectories determined by the fundamental lemma and noisy measurement sequences (see Lemma 2). This trajectory prediction problem defines the lower level problem in our proposed scheme (5), whose single-level reformulation is summarized in Lemma 3. In the end, Section III-C concludes this Section III by comparing the proposed scheme with the existing single-level schemes.

A. Wasserstein Prediction Upper Bound

Regarding (4), the system output \bar{y}_{init} is contaminated by measurement noise, giving a noisy measurement vector y_{init} . The output \bar{y}_{init} , thus, follows the distribution (see Section II-B):

$$\bar{y}_{\text{init}} \sim \mathcal{N}(y_{\text{init}}, \Sigma_{\text{init}})$$

where $\Sigma_{\text{init}} = I_{t_{\text{init}}} \otimes \Sigma_v$. Similarly, the measurement Hankel matrix $\mathfrak{H}_{L,\text{init}}(y_d)$ is subject to measurement noise, and we denote the uncertain system output Hankel matrix by $\mathfrak{H}_{L,\text{init}}(\bar{y}_d)$. Then, for arbitrary $g \in \mathbb{R}^{n_c}$, the following lemma quantifies the distribution distance between an uncertain trajectory generated by the fundamental lemma, $\mathfrak{H}_{L,\text{init}}(\bar{y}_d)g$, and the uncertain system output sequence \bar{y}_{init} .

Lemma 2: $\forall g \in \mathbb{R}^{n_c}$, the squared Wasserstein distance $W(\mathfrak{H}_{L,\text{init}}(\bar{y}_d)g, \bar{y}_{\text{init}})^2$ is upper bounded by

$$\|\mathfrak{H}_{L,\text{init}}(y_d)g - y_{\text{init}}\|^2 + (\sqrt{t_{\text{init}}} \|g\| - 1)^2 \text{tr}(\Sigma_v).$$

Proof: Similar to the distribution of \bar{y}_{init} , the distribution of the i th column of the output Hankel matrix $\mathfrak{H}_{L,\text{init}}(\bar{y})$ follows a Gaussian distribution $\mathcal{N}(y_{d,i:i+t_{\text{init}}-1}, \Sigma_{\text{init}})$, and the adjacent columns are correlated. By the basic properties of Gaussian distributions, we have

$$\mathfrak{H}_{L,\text{init}}(\bar{y}_d)g \sim \mathcal{N}(\mathfrak{H}_{L,\text{init}}(y_d)g, \tilde{\Sigma}_{\text{init}})$$

where $\tilde{\Sigma}_{\text{init}} = \tilde{G} \otimes \Sigma_v$, and the entry of $\tilde{G} \in \mathbb{R}^{t_{\text{init}} \times t_{\text{init}}}$ is

$$\tilde{G}_{i,j} = \sum_{n=1}^{n_c - |i-j|} g_n g_{n+|i-j|}.$$

Hence, the squared Wasserstein distance $W(\mathfrak{H}_{L,\text{init}}(\bar{y}_d)g, \bar{y}_{\text{init}})^2$ is

$$W(\mathfrak{H}_{L,\text{init}}(\bar{y}_d)g, \bar{y}_{\text{init}})^2 = \|\mathfrak{H}_{L,\text{init}}(y_d)g - y_{\text{init}}\|^2 + \underbrace{\text{tr}(\tilde{\Sigma}_{\text{init}} + \Sigma_{\text{init}} - 2(\tilde{\Sigma}_{\text{init}} \Sigma_{\text{init}})^{\frac{1}{2}})}_{(a)}.$$

In the rest of this proof, we will upper bound the term (a) above

$$\begin{aligned} (a) &= \text{tr}(\tilde{\Sigma}_{\text{init}}) + \text{tr}(\Sigma_{\text{init}}) + 2 \text{tr}\left((\tilde{\Sigma}_{\text{init}} \Sigma_{\text{init}})^{\frac{1}{2}}\right) \\ &= (\text{tr}(\tilde{G}) + \text{tr}(I_{t_{\text{init}}})) \text{tr}(\Sigma_v) - 2 \underbrace{\text{tr}\left(((\tilde{G} I_{t_{\text{init}}}) \otimes \Sigma_v^2)^{\frac{1}{2}}\right)}_{(b)} \\ &= t_{\text{init}}(\|g\|^2 + 1) \text{tr}(\Sigma_v) - 2 \underbrace{\text{tr}\left(\tilde{G}^{\frac{1}{2}} \otimes \Sigma_v\right)}_{(c)} \\ &= \left(t_{\text{init}}(\|g\|^2 + 1) - 2 \text{tr}\left(\tilde{G}^{\frac{1}{2}}\right)\right) \text{tr}(\Sigma_v) \\ &\stackrel{(d)}{\leq} \left(t_{\text{init}}(\|g\|^2 + 1) - 2 \text{tr}\left(\tilde{G}\right)^{\frac{1}{2}}\right) \text{tr}(\Sigma_v) \\ &= \left(t_{\text{init}}(\|g\|^2 + 1) - 2\sqrt{t_{\text{init}}} \|g\|\right) \text{tr}(\Sigma_v) \\ &\stackrel{(e)}{\leq} (\sqrt{t_{\text{init}}} \|g\| - 1)^2 \text{tr}(\Sigma_v) \end{aligned} \quad (6)$$

where terms (b) and (c) follow the same fact that $(A \otimes B)(C \otimes D) = AC \otimes BD$. The inequality (d) follows [45, Th. 1 (ii)]

$$\text{tr}(\tilde{G})^{\frac{1}{2}} \leq \text{tr}\left(\tilde{G}^{\frac{1}{2}}\right).$$

The inequality (e) uses the fact that $t_{\text{init}} \geq 1$. We conclude the proof with \blacksquare

$$\begin{aligned} W(\mathfrak{H}_{L,\text{init}}(\bar{y}_d)g, \bar{y}_{\text{init}})^2 &\leq \|\mathfrak{H}_{L,\text{init}}(y_d)g - y_{\text{init}}\|^2 \\ &\quad + (\sqrt{t_{\text{init}}} \|g\| - 1)^2 \text{tr}(\Sigma_v). \end{aligned}$$

Based on the upper bound in Lemma 2, we can generate a trajectory prediction via the following optimization problem:

$$y_{\text{pred}} = \mathfrak{H}_{L,\text{pred}}(y_d)g(\tilde{w}_{\text{pred}}) \quad (7a)$$

$$g(\tilde{w}_{\text{pred}}) \in \arg \min_{g_l, \sigma_l} \frac{1}{2} \|\sigma_l\|^2 + \frac{1}{2} (\sqrt{t_{\text{init}}} \|g_l\| - 1)^2 \text{tr}(\Sigma_v)$$

$$\text{s.t. } \begin{bmatrix} \mathfrak{H}_{L,\text{init}}(y_d) \\ \mathfrak{H}_{L,\text{init}}(u_d) \\ \mathfrak{H}_{L,\text{init}}(\tilde{w}_d) \\ \mathfrak{H}_{L,\text{pred}}(u_d) \\ \mathfrak{H}_{L,\text{pred}}(\tilde{w}_d) \end{bmatrix} g_l = \begin{bmatrix} y_{\text{init}} + \sigma_l \\ u_{\text{init}} \\ \tilde{w}_{\text{init}} \\ u_{\text{pred}} \\ \tilde{w}_{\text{pred}} \end{bmatrix}. \quad (7b)$$

Equation (7b) gives the trajectory expectation generated by Willems' fundamental lemma. Meanwhile, $[y_{\text{init}}^\top + \sigma_l^\top \ u_{\text{init}}^\top \ \tilde{w}_{\text{init}}^\top \ u_{\text{pred}}^\top \ \tilde{w}_{\text{pred}}^\top]^\top$ is the trajectory composed by noisy measurements read out from the sensors, the planned future input, and a predicted disturbance trajectory. Thus, optimization problem (7) minimizes the discrepancy upper bound between an I/O sequence estimated by measurement and an I/O trajectory estimated by the fundamental lemma.

Remark 1: Note that the Hankel matrix $\mathfrak{H}_{L,\text{pred}}(y_d)$ is also subject to measurement noise [v in (4)], which means that the estimate of a fundamental lemma-based predictive trajectory $\mathfrak{H}_{L,\text{pred}}(\bar{y}_d)g$ is also uncertain and Gaussian with expectation $\mathfrak{H}_{L,\text{pred}}(y_d)g$. The prediction given by (7a) can, therefore, be considered as a certainty equivalent prediction. Meanwhile, even though it is possible to consider the uncertainty in y_{pred} , for the sake of a clean layout, we only use the certainty equivalence prediction (7) in this article. It is noteworthy to mention that, based on our experience, the quantified

uncertainty of w_{pred} offered by the weather forecast is usually highly conservative. Using certainty equivalence is empirically sufficient to give desirable robust control performance in building applications (see Section III-B for more details).

B. Tractable Bilevel Reformulation

In this section, we will develop the proposed scheme (5) by integrating the prediction problem (7) into a predictive control problem. This controller should maintain the system performance while ensuring robust constraint satisfaction regardless of future realizations of the process noise, and so we assume that the future process noise \tilde{w}_{pred} can be predicted with uncertainty quantification. Buildings are systems satisfying this assumption. For example, the weather forecast can provide a future temperature prediction with an uncertainty tube centered around a nominal prediction such that the actual future temperature realization fluctuates within this tube. Therefore, we denote the set of predicted future process noise realizations by $\tilde{w}_{\text{pred}} \in \bar{w} \oplus \tilde{\mathcal{W}}$, where \bar{w} is the nominal prediction and $\tilde{\mathcal{W}}$ denotes the uncertainty tube. We state our assumption.

Assumption 2: \bar{w} and $\tilde{\mathcal{W}}$ are known.

To make the controller less conservative, we consider a predictive control input with linear feedback from process noise

$$u_{\text{pred}} = \bar{u}_{\text{pred}} + K \tilde{w}_{\text{pred}} \quad (8)$$

where the feedback control K is a decision variable in our predictive control problem. In particular, \bar{u} reflects the nominal control inputs, while feedback K adapts the control input based on the actual realization of the process noise.

By replacing the lower level problem in (5) [i.e., (5d) and (5c)] with the prediction problem (7), we can state a bilevel robust predictive control problem for LTI systems

$$\min_{\substack{\bar{y}_{\text{pred}} \\ \bar{u}_{\text{pred}}, K}} J(y_{\text{pred}}, u_{\text{pred}}) \quad (9a)$$

s.t. $\forall \tilde{w}_{\text{pred}} \in \bar{w} \oplus \tilde{\mathcal{W}}$

$$u_{\text{pred}} = \bar{u}_{\text{pred}} + K \tilde{w}_{\text{pred}} \in \tilde{\mathcal{U}}$$

$$y_{\text{pred}} = \mathfrak{H}_{L,\text{pred}}(y_{\text{d}})g(\tilde{w}_{\text{pred}}) \in \mathcal{Y}$$

$$g(\tilde{w}_{\text{pred}}) \in \arg \min_{g_l, \sigma_l} \frac{1}{2} \|\sigma_l\|^2 + \frac{1}{2} (\sqrt{t_{\text{init}}} \|g_l\| - 1)^2 \text{tr}(\Sigma_v)$$

$$\text{s.t. } \begin{bmatrix} \mathfrak{H}_{L,\text{init}}(y_{\text{d}}) \\ \mathfrak{H}_{L,\text{init}}(u_{\text{d}}) \\ \mathfrak{H}_{L,\text{init}}(\tilde{w}_{\text{d}}) \\ \mathfrak{H}_{L,\text{pred}}(u_{\text{d}}) \\ \mathfrak{H}_{L,\text{pred}}(\tilde{w}_{\text{d}}) \end{bmatrix} g_l = \begin{bmatrix} y_{\text{init}} + \sigma_l \\ u_{\text{init}} \\ \tilde{w}_{\text{init}} \\ u_{\text{pred}} \\ \tilde{w}_{\text{pred}} \end{bmatrix} \quad (9b)$$

where we set $\tilde{\mathcal{W}} = \mathcal{W}$ and $\tilde{\mathcal{U}} = \mathcal{U}$. Problem (9) is a bilevel optimization problem, whose upper level decides the optimal control and whose lower level generates the corresponding predictive output trajectory. In particular, the upper level problem sends \bar{u}_{pred} and K to the lower level problem. Then, for each specific \tilde{w}_{pred} , the lower level problem returns the corresponding predictor $g(\tilde{w}_{\text{pred}})$, which accordingly defines the output trajectory predictions y_{pred} for that \tilde{w}_{pred} [see (9b)]. In turn, the robust constraint in the upper level ensures that

input and output constraints are satisfied for all \tilde{w}_{pred} in the considered set $\bar{w} \oplus \mathcal{W}$. In conclusion, the upper level problem optimizes \bar{u}_{pred} and K based on the prediction given by the lower level problem.

However, this bilevel problem (9) is hard to solve numerically because the objective in the lower level problem is nonconvex.¹ To address this issue, we state a looser, but convex, Wasserstein upper bound in the following corollary.

Corollary 1: $\forall g \in \mathbb{R}^{n_c}$, the squared Wasserstein distance $W(\mathfrak{H}_{L,\text{init}}(\bar{y}_{\text{d}})g, \bar{y}_{\text{init}})^2$ is upper bounded by

$$\|\mathfrak{H}_{L,\text{init}}(y_{\text{d}})g - y_{\text{init}}\|^2 + t_{\text{init}} \text{tr}(\Sigma_v)(\|g\|^2 + 1).$$

Proof: In the inequality (d) of (6), we have $\text{tr}(\tilde{G}) \geq 0$ as \tilde{G} is positive semidefinite. Therefore, we give a convex Wasserstein distance upper bound as

$$W(\mathfrak{H}_{L,\text{init}}(\bar{y}_{\text{d}})g, \bar{y}_{\text{init}})^2 \leq \|\mathfrak{H}_{L,\text{init}}(y_{\text{d}})g - y_{\text{init}}\|^2 + t_{\text{init}}^2 \text{tr}(\Sigma_v)(\|g\|^2 + 1). \quad \blacksquare$$

Bringing everything together, we eliminate the solution of the nonconvex problem (9) and arrive at a convex tractable version [i.e., the proposed scheme (5)]. This numerically tractable predictive control problem (5) will be used throughout this article. The terms $\tilde{\mathcal{U}}$, $\tilde{\mathcal{W}}$ and \mathcal{E}_g used in the LTI case are given as follows.

- 1) $\mathcal{E}_g = t_{\text{init}}^2 \text{tr}(\Sigma_v)I_{n_c}$: The lower level problem minimizes the convex Wasserstein upper bound given in Corollary 1. For the sake of clarity, the constant term $t_{\text{init}}^2 \text{tr}(\Sigma_v)$ is dropped in its objective.
- 2) $\mathcal{W} = \mathcal{W}$, $\tilde{\mathcal{U}} = \mathcal{U}$: The set of predictive process noise is directly defined by the process noise forecast (see Assumption 2), and the input constraint is not tightened.

Up to this point, we have derived the bilevel structure used in the proposed scheme (5), and we will show that it has a tractable single-level reformulation via the following lemma.

Lemma 3: The following single-level robust optimization problem is equivalent to the bilevel problem (5):

$$\begin{aligned} & \min_{\substack{\bar{y}_{\text{pred}} \\ \bar{u}_{\text{pred}}, K}} J(y_{\text{pred}}, u_{\text{pred}}) \\ \text{s.t. } & \forall \tilde{w}_{\text{pred}} \in \bar{w} \oplus \tilde{\mathcal{W}} \\ & u_{\text{pred}} = \bar{u}_{\text{pred}} + K \tilde{w}_{\text{pred}} \in \tilde{\mathcal{U}} \\ & y_{\text{pred}} = \mathfrak{H}_{L,\text{pred}}(y_{\text{d}})g(\tilde{w}_{\text{pred}}) \in \mathcal{Y} \\ & \begin{bmatrix} g(\tilde{w}_{\text{pred}}) \\ \kappa \end{bmatrix} = M^{-1} \begin{bmatrix} \mathfrak{H}_{L,\text{init}}(y_{\text{d}})^T y_{\text{init}} \\ u_{\text{init}} \\ \tilde{w}_{\text{init}} \\ u_{\text{pred}} \\ \tilde{w}_{\text{pred}} \end{bmatrix} \end{aligned} \quad (10)$$

¹To ensure that a composition of two convex functions is convex, the outer convex function needs to be nondecreasing [15, Ch. 3.2.4]. To see the nonconvexity in (9), one can plot the following function: $f(x) = (|x| - 1)^2$, $x \in \mathbb{R}$.

where κ is the dual variable of (5e) and

$$H := \begin{bmatrix} \mathfrak{H}_{L,\text{init}}(u_{\mathbf{d}}) \\ \mathfrak{H}_{L,\text{init}}(\tilde{w}_{\mathbf{d}}) \\ \mathfrak{H}_{L,\text{pred}}(u_{\mathbf{d}}) \\ \mathfrak{H}_{L,\text{pred}}(\tilde{w}_{\mathbf{d}}) \end{bmatrix} \quad (11a)$$

$$M := \begin{bmatrix} \mathfrak{H}_{L,\text{init}}^{\top}(y_{\mathbf{d}}) & \mathfrak{H}_{L,\text{init}}(y_{\mathbf{d}}) + \mathcal{E}_g & H^{\top} \\ H & \mathbf{O} \end{bmatrix}. \quad (11b)$$

Proof: Note that the uncertain lower level problem in (5) is strongly convex and, therefore, can be equivalently represented by its KKT system [23, Ch. 4]. By replacing σ_l by $\mathfrak{H}_{L,\text{init}}(y_{\mathbf{d}})g_l - y_{\text{init}}$, the Lagrangian of the lower level problem is

$$\begin{aligned} \mathcal{L}(g) = & \frac{1}{2}\|\mathfrak{H}_{L,\text{init}}(y_{\mathbf{d}})g - y_{\text{init}}\|^2 + \frac{1}{2}g^{\top}\mathcal{E}_g g \\ & + \kappa^{\top} \left(Hg - \begin{bmatrix} u_{\text{init}} \\ \tilde{w}_{\text{init}} \\ u_{\text{pred}} \\ \tilde{w}_{\text{pred}} \end{bmatrix} \right) \end{aligned}$$

where κ is the dual variable of the equality constraint. Based on this, we have the stationary condition of the KKT system

$$\begin{aligned} \frac{\partial \mathcal{L}(g)}{\partial g}^{\top} = & (\mathfrak{H}_{L,\text{init}}(y_{\mathbf{d}})^{\top} \mathfrak{H}_{L,\text{init}}(y_{\mathbf{d}}) + \mathcal{E}_g)g + H^{\top}\kappa \\ & - \mathfrak{H}_{L,\text{init}}(y_{\mathbf{d}})^{\top}y_{\text{init}} = 0. \end{aligned}$$

By recalling the primal feasibility condition

$$Hg = \begin{bmatrix} u_{\text{init}} \\ \tilde{w}_{\text{init}} \\ u_{\text{pred}} \\ \tilde{w}_{\text{pred}} \end{bmatrix}$$

we get the uncertain KKT matrix M in (11b). Finally, by Assumption 1, M is full-rank and, hence, invertible [46, Ch. 16]. This leads to the uncertain KKT equation (10), which concludes the proof. ■

On top of the single-level problem (10), we further enforce causality on the decision variable K through a lower block triangular structure [36, Ch. 5.1]

$$K = \begin{bmatrix} \mathbf{O} & \mathbf{O} & \mathbf{O} & \dots & : \\ K_{2,1} & \mathbf{O} & \mathbf{O} & \dots & : \\ K_{3,1} & K_{3,2} & \mathbf{O} & \dots & : \\ \vdots & \ddots & \ddots & \ddots & : \\ K_{n_h,1} & K_{n_h,2} & K_{n_h,3} & \dots & \mathbf{O} \end{bmatrix}. \quad (12)$$

In particular, causality means that the i th step of the future process noise can only change the events happening later than it, which only includes the $i+1$ th to the n_h th components in u_{pred} .

Remark 2: When the feasible sets $\tilde{\mathcal{U}}, \mathcal{Y}$ are polytopic, the robust optimization problem (10) can be solved by a standard dualization procedure [7].

C. Discussion

We would wrap up this Section III by a comparison between the proposed scheme and existing single-level schemes. Based on Willems' fundamental Lemma 1, a data-driven control scheme has been proposed in [19] and [41]

$$\min_{g, \sigma} \underbrace{J(y_{\text{pred}}, u_{\text{pred}})}_{(a)} + \underbrace{\eta_g\|g\| + \eta_{\sigma}\|\sigma\|}_{(b)} \quad (13a)$$

$$\text{s.t. } \begin{bmatrix} \mathfrak{H}_{L,\text{init}}(y_{\mathbf{d}}) \\ \mathfrak{H}_{L,\text{init}}(u_{\mathbf{d}}) \\ \mathfrak{H}_{L,\text{pred}}(u_{\mathbf{d}}) \\ \mathfrak{H}_{L,\text{pred}}(y_{\mathbf{d}}) \end{bmatrix} g = \begin{bmatrix} y_{\text{init}} + \sigma \\ u_{\text{init}} \\ u_{\text{pred}} \\ y_{\text{pred}} \end{bmatrix} \quad (13b)$$

$$u_{\text{pred}} \in \mathcal{U}, \quad y_{\text{pred}} \in \mathcal{Y}$$

where η_g and η_{σ} are user-defined parameters and other components are similar to those defined in the proposed scheme (5). For the sake of clarity, we neglect the process noise in this subsection. By comparing its objective (13a) with the objective function in the lower level problem [i.e., (5d)], one can see that the last two terms (b) can be understood as the penalty on prediction error. These regularization terms are studied in [21] and [25]. In particular, [25] shows that the first term in (b) is linked to the objective function used in the standard system identification procedure. Therefore, problem (13) can be understood as a biobjective optimization problem, whose loss function tries to balance the prediction accuracy and control performance. Such a tradeoff between these two objectives is modeled into the user-defined weights η_g and η_{σ} . However, based on our experiments and the results reported in [19], [24], [28], and [32], the tuning of η_g and η_{σ} usually requires exhaustive search and is in general nontrivial. Instead of balancing the prediction accuracy and the control performance in a single objective function (13a), the proposed scheme couples them hierarchically in a bilevel optimization problem (5). This follows an intuitive logic applied in predictive control: the control is decided based on an accurate output prediction. In the proposed scheme (5), the prediction accuracy is optimized directly by the lower level problem. Thus, the prediction accuracy of the output trajectory is always guaranteed without sacrificing the control optimality (i.e., upper level objective). On the other hand, the prediction accuracy of the single-level scheme (13) might be compromised due to the tradeoff between control performance and the prediction accuracy (i.e., terms (a) and (b) in objective (13a), respectively). To better see why the proposed scheme is preferable, one can consider a special case where $\mathcal{Y} = \mathbf{0}$, $\mathcal{U} = \mathbf{0}$ and $u_{\text{init}} = \mathbf{0}$. In this case, problem (13) has a nonempty solution set as $g = 0$ is feasible regardless of the value of y_{init} . This solution corresponds to an output trajectory that can jump to the origin in one step with zero input regardless of the initial state. If we do not consider the case where $A_i = \mathbf{O} \forall i$ [see dynamics (4)], the underlying dynamics are not able to follow this predicted trajectory for arbitrary y_{init} , and hence, the prediction can be inconsistent in the single-level scheme (13). In comparison, because the prediction accuracy is independently ensured by the lower level problem, the proposed scheme (5) will be infeasible unless the initial state is at the origin. In practice, the corner case given above barely happens; as reported by

Coulson et al. [20] and Dörfler [24], it is always possible to tune η_g and η_σ to achieve a desirable closed-loop performance. Note that, when the regularization term (b) in (13a) is not quadratic, its corresponding bilevel will be more difficult to solve numerically, as there is no convex single-level reformulation. Hence, whether one uses the proposed bilevel structure or not depends on the specific application.

Remark 3: The idea of bilevel optimization is also presented in [25] and in subspace predictive control (SPC) [30]. In these previous works, the lower level problem defines a system identification problem based on the historical data (i.e., $\{u_d, y_d\}$). These approaches try to identify one single model, which is a preprocessed historical dataset in [25] (see Problem (5) and (20) in [25]), and an ARX model in SPC. Thus, in this identification setup, the treatment of the noise presented in the online measurements (e.g., noise in y_{init}) is independent of the treatment of the measurement noise presented in the historical data (i.e., the identification problem). On the contrary, our proposed scheme deals with these two sources of measurement noise in a more unified way. First, because of the noise in the historical data, the representation of the underlying dynamics is uncertain. In the proposed scheme, all the possible representations are considered (i.e., the uncertain Hankel matrices considered in Section III-A). Second, both the uncertain representations and the online measurement noise are treated in one single problem via a Wasserstein distance upper bound (see Corollary 1). Due to these differences, we intentionally call the lower level problem in the proposed scheme a “trajectory prediction” problem but not an “identification” problem.

Remark 4: Different from our analysis, Coulson et al. [21] study a general setup that further includes unknown process noise. Coulson et al. [21] apply the Wasserstein distance to show that the regularization on g [first term of (b) in (13a)] is related to the minimization of the conditional value at risk (CVaR) from a distributionally robust viewpoint.

Remark 5: The objective function $J(y_{\text{pred}}, u_{\text{pred}})$ has different choices, such as the robust objective $J(y_{\text{pred}}, u_{\text{pred}}) = \max_{\tilde{w}_{\text{pred}}} \tilde{J}(y_{\text{pred}}, u_{\text{pred}})$. However, unless $\tilde{J}(\cdot, \cdot)$ is linear, this robust objective is nonconvex and, therefore, does not meet our requirement (see Section II-B). Notice that the certainty equivalence is widely adopted in building applications; it is, therefore, reasonable to optimize the nominal performance (i.e., $J(y_{\text{pred}}, u_{\text{pred}}) = \tilde{J}(\bar{y}_{\text{pred}}, \bar{u}_{\text{pred}})$).

IV. HEURISTIC TIME-VARYING EXTENSION

In this section, we will adapt the controller (5) to LTV dynamics (4) by two heuristics. The modifications are summarized as follows.

- 1) *Modification of the Lower Level Objective:* \mathcal{E}_g is a diagonal matrix $\text{diag}(\eta_{g,1}, \dots, \eta_{g,n_c})$, and the weight sequence $\{\eta_{g,i}\}_{i=1}^{n_c}$ is decreasing. Recall that the i th entry of g , g_i , is the weight of the i th column in H and $\mathfrak{H}_{L,\text{init}}(y_d)$ used for prediction. Thus, a nonuniform penalty on g can be used to model our preference of using recent data for trajectory prediction, and the decreasing diagonal elements in \mathcal{E}_g reflect this preference.

- 2) *Adaptation of the Measured Dataset:* The data are updated online to capture the latest dynamics from the system. In particular, Hankel matrices are updated by appending new input/output measurements on the right-hand side of the Hankel matrices and discarding old data on the left-hand side.

Note that the second heuristic is tailored for slowly time-varying systems. This is the case for building applications, whose variations are usually seasonal. This section will discuss how to update the dataset in a way that can robustly guarantee the data quality (see Section IV-A) and that has a scalable update computation (see Section IV-B). It is worth mentioning that updating the dataset online is also used in [12] to learn the linearized model around different operating points online.

A. Active Excitation

In this part, we will discuss the selection of $\tilde{\mathcal{U}}$ and $\tilde{\mathcal{W}}$ in (5). Recall that persistent excitation is the key assumption required for Willems’ fundamental lemma to apply. As the persistent excitation condition is not explicitly considered in the predictive control problem (5), thus, the control input excitation may become impersistent in the closed loop. In this case, updating Hankel matrices with this latest I/O sequence is not reasonable. For example, in building control, if the outdoor temperature and/or solar irradiation are near the building’s equilibrium point, no extra heating/cooling is needed when the energy consumption is aimed to be minimized. In this case, the long-term zero-valued control input will not excite the system persistently. To accommodate this issue, we introduce a robust active excitation scheme, which perturbs the control input applied at time i by a random excitation signal

$$u_i = \underbrace{\bar{u}_{\text{pred},1|i}}_{(a)} + \underbrace{u_{e,i}}_{(b)} \quad (14)$$

where $\bar{u}_{\text{pred},1|i}$ is the first element of \bar{u}_{pred} determined by a predictive control problem (5) solved at time i . In this decomposition, the term (a) is determined by the predictive control problem (5) with some specific choice of $\tilde{\mathcal{U}}$ and $\tilde{\mathcal{W}}$ (see Algorithm 1), and the term (b) is a bounded excitation input, which is unknown to the decision process of $\bar{u}_{\text{pred},1|i}$. More specifically, from the viewpoint of u_{pred} , u_e is an uncontrolled, but measurable, process noise, and the underlying time-varying linear dynamics, therefore, becomes

$$x_{i+1} = A_i x_i + B_i u_{\text{pred},1|i} + [E_i \quad B_i] \begin{bmatrix} w_i \\ u_{e,i} \end{bmatrix}$$

where the excitation input is randomly sampled from a user-defined compact set as $u_e \in \mathcal{U}_e \subset \mathcal{U}$. The process noise \tilde{w} is accordingly augmented to $[w_{\text{pred}}^\top \quad u_e^\top]^\top$, and the uncertainty set $\tilde{\mathcal{W}}$ in (5a) is augmented to $(\bar{w} \oplus \mathcal{W}) \times \mathcal{U}_e$. As a result, \tilde{w}_{init} is set to $[w_{\text{init}}^\top \quad \mathbf{0}^\top]^\top$. Meanwhile, due to an extra excitation signal in (14), the feasible set of the control input $\tilde{\mathcal{U}}$ is tightened to $\mathcal{U} \ominus \mathcal{U}_e$.

In practice, this active excitation mechanism sacrifices the flexibility of the control input for data quality. If not necessary, we should set $\tilde{\mathcal{U}} = \mathcal{U}$ and $\tilde{\mathcal{W}} = \mathcal{W}$ to generate control inputs and deactivate the active excitation scheme. We summarize the

Algorithm 1

```

while true do
    Measure  $\bar{y}_i, w_i$  and update Hankel matrices.
     $\tilde{\mathcal{U}} \leftarrow \mathcal{U}, \tilde{\mathcal{W}} \leftarrow \bar{w} \oplus \mathcal{W}$ 
    Solve problem (5) to get  $\bar{u}_{\text{pred}|i}$ 
    if input excitation  $\{u_d, \bar{u}_{\text{pred}|i}\}$  is not persistently exciting
        then
             $\tilde{\mathcal{U}} \leftarrow \mathcal{U} \ominus \mathcal{U}_e, \tilde{\mathcal{W}} \leftarrow (\bar{w} \oplus \mathcal{W}) \times \mathcal{U}_e$ 
            Solve problem (5) to get  $\bar{u}_{\text{pred}|i}$ 
            Sample  $u_{e,i}$  from  $\mathcal{U}_e$ 
            Apply  $u_i = \bar{u}_{\text{pred},1|i} + u_{e,i}$ 
        else
            Apply  $u_i = \bar{u}_{\text{pred},1|i}$ 
        end if
         $i \leftarrow i + 1$ 
end while

```

general algorithm of the proposed controller in Algorithm 1, which automatically selects the uncertainty set $\tilde{\mathcal{W}}$ and input feasible set $\tilde{\mathcal{U}}$.

In this algorithm, problem (10) is first solved without active excitation. If its nominal solution \bar{u}_{pred} is not expected to be persistently excited, problem (10) is resolved considering the active excitation scheme. Note that the computational cost of checking the rank condition is $O(n_c^3)$ [50] and may not be affordable for online computation. This can be replaced by some effective heuristics. In building control, the control input excitation becomes impersistent mainly when the control input is zero (e.g., when the cooling/heating is turned off), and thus, the persistence excitation condition can be heuristically replaced by checking whether the nominal predictive input is near to a zero-valued sequence up to some user-defined tolerance. This heuristic is particularly useful in building control. Because when input is not zero-valued, the stochastic property of the process noise (e.g., solar radiation and outdoor weather) will cause random fluctuation in the closed-loop input trajectory, and the persistent excitation condition is, in turn, satisfied. On top of this aspect, due to the stochastic property of the process noise, the process noise is usually persistently excited.

Remark 6: In general, generating a persistently excited control input while considering control performance is challenging, as the persistent excitation condition depends on the rank of $\mathfrak{H}_L(u_d)$, which turns the optimization problem into a challenging nonsmooth nonconvex optimization [39]. It is noteworthy that Faradonbeh et al. [29] also perturb the nominal control input to guarantee persistent excitation; however, their result has no guarantee of robust constraint satisfaction.

Remark 7: Due to the causality constraints in (12), the matrix K in (5b) cannot instantaneously counteract the excitation signal u_e with a $K = [K_w \ -I]$, which is noncausal.

B. Numerical Details

In our proposed adaptive robust controller, the Hankel matrices are updated online with the real-time measurement of u_i, y_i, w_i (see Section IV and Algorithm 1). Meanwhile,

a numerically efficient reformulation of the robust problem (10) requires an explicit evaluation of matrix inversion M^{-1} in (10) at each update. More specifically, when the feasible sets $\tilde{\mathcal{U}}, \mathcal{Y}$ and the uncertainty set $\tilde{\mathcal{W}}$ are polytopic or ellipsoidal, the dualization/explicit upper bound of the robust inequality constraint depends on the matrix inversion M^{-1} . However, the computational cost of M^{-1} is $O((n_c + n_r)^3)$ [50] with n_r and n_c being the number of rows and columns in the matrix H , which is roughly cubic in the size of the dataset. Thus, the direct inverse of M online is not scalable. This is particularly important for building applications because the computing unit in building applications is usually of lower performance [51]. We, therefore, propose to apply two linear algebraic techniques to resolve this computational bottleneck.

Notice that the dual variable κ in the lower problem does not affect the upper level problem. For the sake of compactness, we denote $M_{1,1} := \mathfrak{H}_{L,\text{init}}^\top(y_d) \mathfrak{H}_{L,\text{init}}(y_d) + \mathcal{E}_g$ and $M_{\text{sch}} := (HM_{1,1}^{-1}H^\top)^{-1}HM_{1,1}^{-1}$. By matrix inversion of a block-structured matrix, we have

$$M^{-1} = \begin{bmatrix} M_{1,1}^{-1} - M_{1,1}^{-1}H^\top M_{\text{sch}} & M_{\text{sch}}^\top \\ M_{\text{sch}} & -(HM_{1,1}^{-1}H^\top)^{-1} \end{bmatrix}.$$

We can, therefore, replace the constraint (10) by

$$g(\tilde{w}_{\text{pred}}) = M_{\text{top}} \begin{bmatrix} \mathfrak{H}_{L,\text{init}}(y_d)^\top y_{\text{init}} \\ u_{\text{init}} \\ \tilde{w}_{\text{init}} \\ u_{\text{pred}} \\ \tilde{w}_{\text{pred}} \end{bmatrix}$$

where

$$M_{\text{top}} := [M_{1,1}^{-1} - M_{1,1}^{-1}H^\top M_{\text{sch}} \quad M_{\text{sch}}].$$

With the aforementioned modification, the computational cost is lowered to $O(n_c^3)$, whose computational bottleneck lies at the inversion of $M_{1,1}$. We further lower the computational cost by the Woodbury matrix identity

$$\begin{aligned} M_{1,1}^{-1} &= (\mathfrak{H}_{L,\text{init}}^\top(y_d) \mathfrak{H}_{L,\text{init}}(y_d) + \mathcal{E}_g)^{-1} \\ &= \mathcal{E}_g^{-1} - \mathcal{E}_g^{-1} \mathfrak{H}_{L,\text{init}}^\top(y_d) M_{\text{mid}}^{-1} \mathfrak{H}_{L,\text{init}}(y_d) \mathcal{E}_g^{-1} \end{aligned} \quad (15)$$

where $M_{\text{mid}} := I_m + \mathfrak{H}_{L,\text{init}}(y_d) \mathcal{E}_g^{-1} \mathfrak{H}_{L,\text{init}}^\top(y_d)$. As \mathcal{E}_g is diagonal with a simple and explicit inversion, the major computation cost happens at the inversion of a size m matrix M_{mid} , where $m := t_{\text{init}} n_y$. Thus, the computational cost of $M_{1,1}^{-1}$ and M_{top} is lowered to $O(m^3)$, which is fixed and independent of the number of columns in the Hankel matrices (i.e., roughly the size of the dataset).

Remark 8: Note that the KKT matrix is usually ill-conditioned [46, Ch. 16]. Replacing the full matrix inversion in (10) with the proposed techniques can improve the numerical stability. Because only the matrix inversion of \mathcal{E}_g and M_{mid} in (15) is evaluated, these two matrices are well-conditioned.

V. NUMERICAL RESULTS

In this part, we will demonstrate that our proposed scheme shows comparable performance against some model-based methods in both LTI and LTV systems.

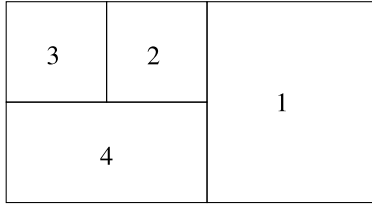


Fig. 1. Schematic of the multizone building.

A. Multizone Building Model

It should be noted that we are not claiming that the data-driven approach outperforms all model-based approaches, as it is definitely possible to tune a better model-based method, such as considering the uncertainty of the identified parameters or using a more complex estimator/controller. We only aim to show that the proposed approach has comparable performance against a model-based method but without requiring a model. We, therefore, select a standard model-based controller design pipeline that we believe is reasonable, and we compare this standard scheme against our proposed scheme in this example. We considered an LTI multizone building model reported in [6] (indices of the rooms are shown in schematic Fig. 1). Due to the space limit, the parameters of the model (i.e., A , B , C , D , and E matrices) are included in the Supplementary Material on GitHub.² In this multizone building (see Fig. 1), room 4 is the corridor linking a large warehouse (room 1) and two offices (room 2 and 3). The indoor temperature of room 1 is controlled by an independent HVAC system, while another HVAC controls the temperature of all other rooms (i.e., $u \in \mathbb{R}^2$). Only the indoor temperature of these four rooms is measured (i.e., $y \in \mathbb{R}^4$), while the underlying model is 13-D, including the wall temperature (i.e., $x \in \mathbb{R}^{13}$). Process noises are outdoor temperature and solar radiation (i.e., $w \in \mathbb{R}^2$), and real weather data are used for the closed-loop simulation. The sampling time of this discrete-time model is 15 min. Recall the system dynamics (4); two different levels of unknown measurement noise v are considered to show the reliability of the proposed scheme. We remind the reader that only the measurement y_i is available to both schemes, and \bar{y}_i is unknown to both schemes [see the dynamics (4)].

In the “standard” scheme, the model is identified by a subspace identification algorithm, and the state estimation is done by a Kalman filter.³ Following this, a robust model predictive controller with linear feedback [36] is used in the “standard” scheme to generate control inputs⁴

$$\begin{aligned} & \min_{\substack{u_{\text{pred}}, K_w \\ y_{\text{pred}}}} J(\bar{y}_{\text{pred}}, \bar{u}_{\text{pred}}) \\ \text{s.t. } & x_{\text{pred},0} = x_0 \\ & \forall i = 0, 1, \dots, n_h \\ & x_{\text{pred},i+1} = A_{id}x_{\text{pred},i} + B_{id}u_{\text{pred},i} \end{aligned}$$

²https://github.com/YingZhaoLeo/Building_results

³We use the commands N4SID and KALMAN in MATLAB to do subspace identification and Kalman filter design, respectively.

⁴We used the code template of “approximate closed-loop minimax solution” in <https://yalmp.github.io/example/robustmpc>

TABLE I
STATISTICS OF THE CONSTRAINT VIOLATION AND THE FITTING ACCURACY OF THE IDENTIFIED MODELS. THE BRACKET NUMBER IN EACH ENTRY CORRESPONDS TO THE TESTS WHOSE STANDARD DEVIATION OF MEASUREMENT NOISE IS 0.3°C , AND THE UNBRACKETED ONES ARE OF 0.05°C MEASUREMENT NOISE STANDARD DEVIATION

Room index	1	2	3	4	
Constraint violation	Proposed scheme	0.67% (3.12%)	0% (0.14%)	0.40% (2.76%)	0% (0.078%)
	Standard scheme	2.78% (11.46%)	0% (0.99%)	3.28% (10.27%)	0.42% (3.77%)
	Averaged fitting accuracy	93.17% (77.60%)	93.07% (73.43%)	90.72% (71.32%)	92.58% (83.93%)

$$\begin{aligned} & + E_{id}w_{\text{pred},i} \\ y_{\text{pred},i} & = C_{id}x_{\text{pred},i} + D_{id}u_{\text{pred},i} \\ \forall w_{\text{pred}} \in \mathcal{W}, \quad u_{\text{pred}} & = \bar{u}_{\text{pred}} + K_w w_{\text{pred}} \\ u_{\text{pred}} \in \mathcal{U}, \quad y_{\text{pred}} & \in \mathcal{Y} \end{aligned} \quad (16)$$

where the parameters of A_{id} , B_{id} , E_{id} , C_{id} , and D_{id} come from system identification and x_0 is estimated with a Kalman filter. Note that the feedback control law K_w is optimized by (16). Other components, such as $J(\cdot, \cdot)$, n_h , and $\mathcal{U}, \mathcal{Y}, \mathcal{W}$, are identical to those used in the proposed robust data-driven scheme. In particular, the heating power (control input) $0 \text{ kW} \leq u_{\text{pred}} \leq 4.5 \text{ kW}$, the indoor temperatures for all the rooms are bounded within $20^\circ\text{C} \leq y_{\text{pred}} \leq 26^\circ\text{C}$, and the uncertainty of the solar radiation and the outdoor temperature prediction are modeled by a tube around their nominal prediction. The radii of the tube are, respectively, 2 kW/m^2 and 2°C , and the nominal prediction $\bar{w}_{\text{pred},i}$ comes from the weather forecast. An indoor temperature control problem is considered

$$J(y_{\text{pred}}, u_{\text{pred}}) = \sum_{i=0}^{n_h} 10(\bar{y}_{\text{pred},i+1} - y_{\text{ref}})^2 + 0.1\bar{u}_{\text{pred},i}^2$$

where y_{ref} is the set-point of the indoor temperature, the prediction horizon is set to $n_h = 8$, and the sampling time of this model is 15 min. In addition, we set $t_{\text{init}} = 5$ in the proposed robust scheme. To ensure a fair comparison, the same dataset is used for system identification and for defining the Hankel matrices in the LTI case and the initial Hankel matrices in the LTV case. Four days of historical data are used, which includes 384 datapoints.

Two experiments with different levels of measurement noise are considered, whose standard deviations are, respectively, 0.05°C and 0.3°C . These two cases correspond to a measurement error roughly bounded by 0.15°C and 1°C , respectively. The results are shown in Fig. 2⁵ and Table I. Each experiment carries out 50 Monte Carlo runs. In each Monte Carlo run, a new dataset is generated for system identification and the definition of the Hankel matrices. The averaged fitting accuracy⁶ is summarized in Table I as well, which shows good

⁵To be fair, both controllers are subject to the same measurement noise and process noise during their online operation.

⁶The fitting accuracy is generated by the COMPARE command in MATLAB.

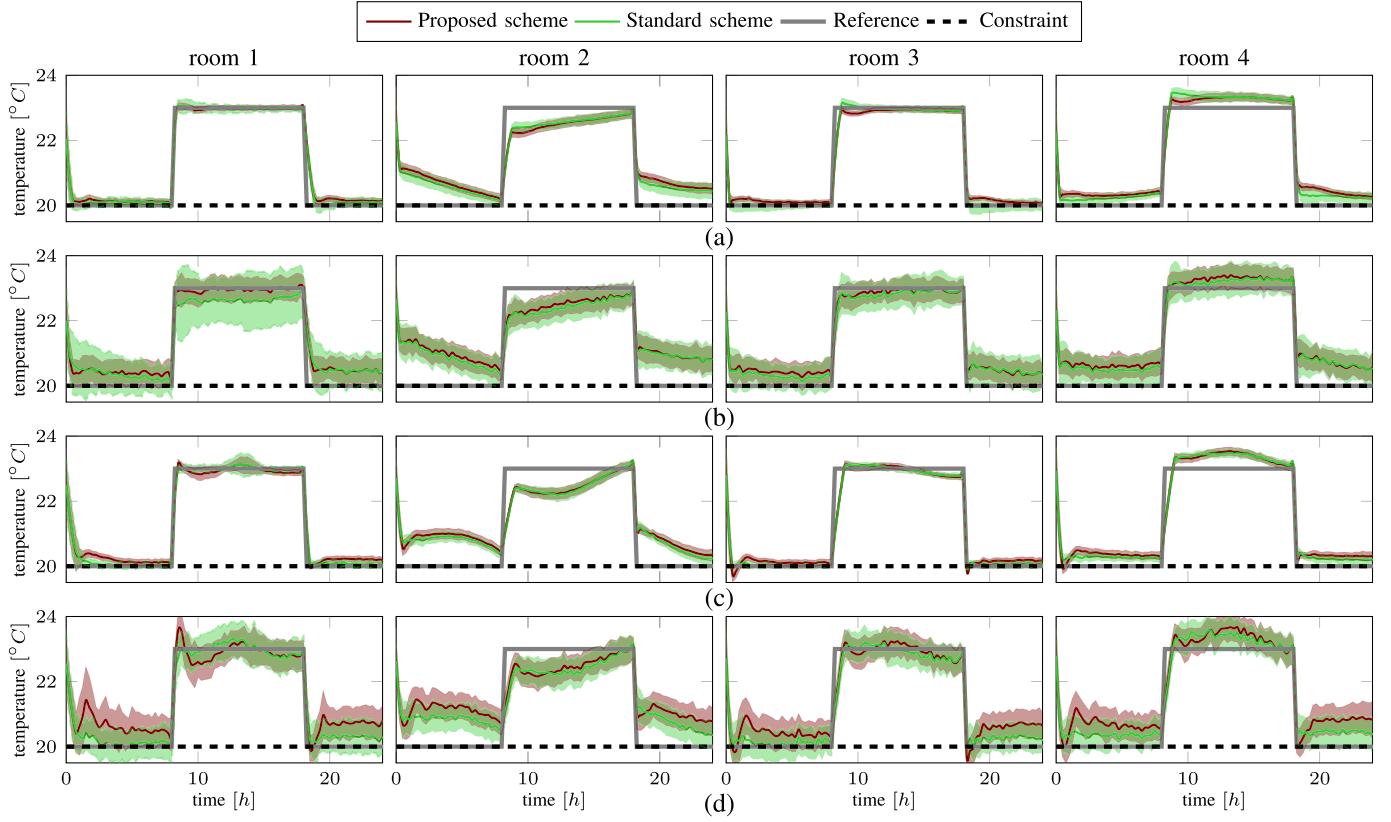


Fig. 2. Comparison of the proposed data-driven control and the model-based controller. The shaded region is the mean \pm two standard deviations of all Monte Carlo runs. Std of measurement noise: row (a): LTI model, measurement noise std: $0.05\text{ }^{\circ}\text{C}$; row (b): LTI model, measurement noise std: $0.3\text{ }^{\circ}\text{C}$; row (c): LTV model, measurement noise std: $0.05\text{ }^{\circ}\text{C}$; and row (d): LTV model, measurement noise std: $0.3\text{ }^{\circ}\text{C}$.

modeling accuracy in the “standard” scheme. In addition, the constraint violation is calculated by

$$\frac{\text{number of steps where a constraint violation occurs}}{(\text{number of simulation steps} \times \text{number of Monte Carlo runs})}.$$

From the rows (a) and (b) in Fig. 2, we can observe that the proposed scheme shows comparable performance against the model-based scheme. Meanwhile, when the measurement noise is larger, the variance of the closed-loop trajectory is higher in the data-driven scheme and the model-based scheme. This also leads to more frequent constraint violations. While both controllers violate the constraints more frequently in this case, our proposed scheme offers a better constraint satisfaction guarantee. The constraint violation statistics are summarized in Table I, and we observe that our proposed controller offers much better constraint satisfaction. In the proposed scheme, constraint violations are caused by the reason discussed in Remark 1. On the other hand, we believe that the constraint violation in the model-based method can be resolved by more complex methods, such as constraint tightening, but there is currently no systematic way to achieve this. Last but not least, in the comparison with the single-level scheme, the proposed scheme shows a lower variance in the closed-loop operation, which leads to higher constraint satisfaction, when the measurement noise is higher.

In the second test, we consider that the building dynamics vary slowly on a weekly basis

$$A_i = A + 0.02 \sin\left(\frac{i\pi}{336}\right)I_{13} \\ B_i = B, \quad C_i = C, \quad D_i = D, \quad E_i = E \quad \forall i.$$

Our proposed scheme is compared against a model-based adaptive method, where a recursive least square (RLS) estimator updates the parameter of an ARX model

$$y_i = \sum_{j=1}^{t_{\text{init}}} \theta_{y,j}^\top y_{i-j} + \theta_{u,j}^\top u_{i-j} + \theta_{w,j}^\top w_{i-j}$$

where $\theta_{y,j} \in \mathbb{R}^4$, $\theta_{u,j} \in \mathbb{R}^2$, $\theta_{w,j} \in \mathbb{R}^2$. The model estimated by RLS is used in the following robust MPC problem:

$$\begin{aligned} & \min_{u_{\text{pred}}, K_w} \max_{y_{\text{pred}}} J(y_{\text{pred}}, u_{\text{pred}}) \\ & \text{s.t. } x_{\text{pred},0} = x_0 \\ & \quad \forall i = 0, 1, \dots, n_h \\ & \quad y_{\text{pred},i} = \sum_{j=1}^{t_{\text{init}}} \theta_{y,j} y_{\text{pred},i-j} + \theta_{u,j} u_{\text{pred},i-j} \\ & \quad + \theta_{w,j} w_{\text{pred},i-j} \\ & \quad \forall w_{\text{pred}} \in \mathcal{W}, \quad u_{\text{pred}} = \bar{u}_{\text{pred}} + K_w w_{\text{pred}} \\ & \quad u_{\text{pred}} \in \mathcal{U}, \quad y_{\text{pred}} \in \mathcal{Y} \end{aligned} \quad (17)$$

TABLE II
STATISTIC OF THE CONSTRAINT VIOLATION. THE BRACKET NUMBER IN EACH ENTRY CORRESPONDS TO THE TESTS WHOSE STANDARD DEVIATION OF MEASUREMENT NOISE IS $0.3\text{ }^{\circ}\text{C}$, AND THE UNBRACKETED ONES ARE OF $0.05\text{ }^{\circ}\text{C}$ MEASUREMENT NOISE STANDARD DEVIATION

	room index	1	2	3	4
Constraint violation	Proposed scheme	1.64% (6.99%)	0% (0.49%)	2.70% (7.65%)	0.47% (2.25%)
	RLS-MPC scheme	8.23% (22.54%)	0.37% (3.08%)	10.16% (22.21%)	0.69% (11.11%)



Fig. 3. Polydome.

where the parameters θ_y , θ_u , and θ_w are updated by the RLS estimator. Other settings are the same as the previous experiments. In particular, the RLS estimator has a forgetting factor of 0.98, and it is initialized by the data used to build the initial Hankel matrices of the proposed scheme. Two experiments with different levels of measurement noise standard deviation are conducted. The results are shown in rows (c) and (d) in Fig. 2, and the constraint violation statistics are given in Table II. From rows (c) and (d) in Fig. 2, we can see that both approaches perform the tracking task properly, and the proposed scheme shows comparable performance against the RLS-MPC approach. One major observation is that the proposed scheme shows better constraint satisfaction against the RLS-MPC method. Indeed, it is possible to consider the uncertainty generated by the RLS estimator to improve the robustness of the model-based approach; however, it turns out to be a nonconvex robust optimization problem, and there is no standard approach to solve this problem.

VI. EXPERIMENT

This part presents our real-world experiments conducted at a conference building on the École Polytechnique Fédérale de Lausanne (EPFL) campus.

A. Experimental Setup

The building control experiment is conducted on an entire building, which is a freestanding 600 m^2 single-zone building on the EPFL campus, called the *Polydome*. It is regularly used for lectures/exams and accommodates up to 200 people (see Fig. 3).

In the presented experiments, the indoor temperature measurement is the noisy output measurement y , the active electrical energy consumption of the HVAC system is the input u , and the weather conditions (outdoor temperature and

solar radiation) are the process noise $w = [w_1 \ w_2]$. The sampling period T_s is 15 min, and the structure of the control system is depicted in Fig. 4, where the arrows indicate the direction of data transmission. The system consists of five main components.

- 1) *Sensors*: Four Z-wave FIBARO DOOR/WINDOW SENSORS V2 are put in different locations in the *Polydome* to measure the indoor temperature (path (a)). Every 5 min, the temperature measurements are sent to the database through a wireless Z-wave network [path (c)]. The average value of the four measurements is used as the indoor temperature. The active power consumption of the HVAC system is measured via an EMU three-phase power meter [1] [path (b)].
- 2) *Database*: We use INFLUXDB 1.3.7 [2] to log the time-series data, which records the measurements from sensors [path (c)], the control input computed from the PC [path (d)], and the historical weather [path (f)].
- 3) *Weather API*: We use TOMORROW.IO [3], which provides both historical and current measurements of solar radiation and outdoor temperature to the database [path (f)]. It also provides the forecast of solar radiation and outdoor temperature to the PC to solve the predictive control problem [path (g)].
- 4) *Controller*: The controller is implemented in MATLAB, interfacing YALMIP [37], which fetches historical data from the database to build/update the Hankel matrices [path (d)] and acquires weather forecasts from the weather API [path (g)]. It runs Algorithm 1 to generate the control input. This control signal is transmitted to the HVAC system via the serial communication protocol, Modbus [53].
- 5) *HVAC*: A roof-top HVAC unit (series No: AERMEC RTY-04 heat pump) is used for heating, cooling, and ventilation. Its heating and cooling units are different, consisting of two compressors for heating and one compressor for cooling, respectively.

The HVAC system is shipped with an internal hierarchical controller, which includes the following.

- 1) *Mode Scheduler*: The scheduler determines whether the HVAC is in heating or cooling mode, and we are not authorized to access this scheduler.
- 2) *Temperature Controller*: The indoor temperature is controlled by a bang-bang controller that compares the set-point temperature and the return-air (indoor) temperature with a dead band of $1\text{ }^{\circ}\text{C}$. For example, in the heating mode, if the return-air temperature is $1\text{ }^{\circ}\text{C}$ lower than the set-point temperature, the heating will turn on and run at full power of 8.4 kW until the set-point is reached, and vice versa for cooling, except that the electric power is 7 kW .

To map this controller to our proposed controller, we applied the following strategies.

- 1) As the cooling and heating modes of the HVAC system show different responses, two different I/O datasets for different modes are maintained/updated independently. The controller monitors the mode of the HVAC system

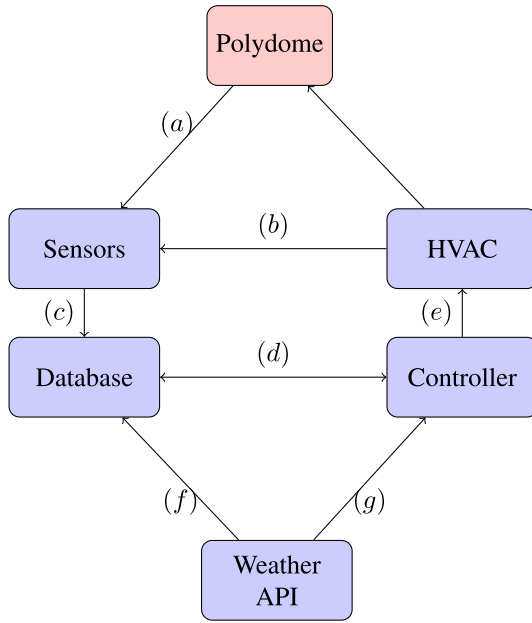


Fig. 4. Structure of the building control system.

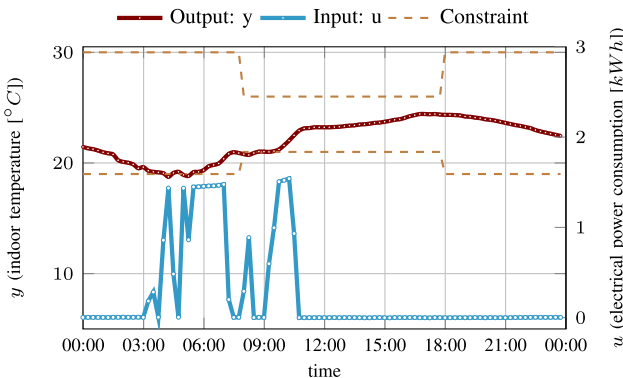


Fig. 5. First experiment in Polydome: one-day heating-mode running by the bilevel data-driven control without robust optimization.

and deploys the corresponding I/O dataset to build the proposed controller.

- Recall that the input used in our proposed scheme is electrical energy consumption. To achieve a desired power consumption, we convert this desired consumption to a set-point sequence: For example, if the HVAC is in heating mode, and a nonzero desired power consumption is planned, the controller will turn on the heating by giving a set-point that is 2°C above the return-air temperature, until the desired energy ($P_{\text{el}}T_s$) is reached (path (b) in Fig. 4). Then, the heating is turned off by setting the set-point to the return-air temperature.

In our bilevel predictive control scheme, the Hankel matrices for both heating and cooling modes are built from 200 datapoints, with $t_{\text{init}} = 10$ and a prediction horizon $n_h = 10$. The controller minimizes electrical power consumption with the following loss function:

$$J(y_{\text{pred}}, u_{\text{pred}}) = \sum_i |\bar{u}_i|.$$

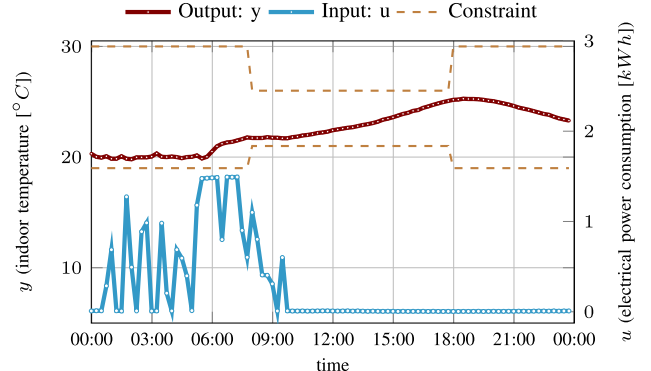


Fig. 6. First experiment in Polydome: one-day heating-mode running by the proposed robust data-driven control.

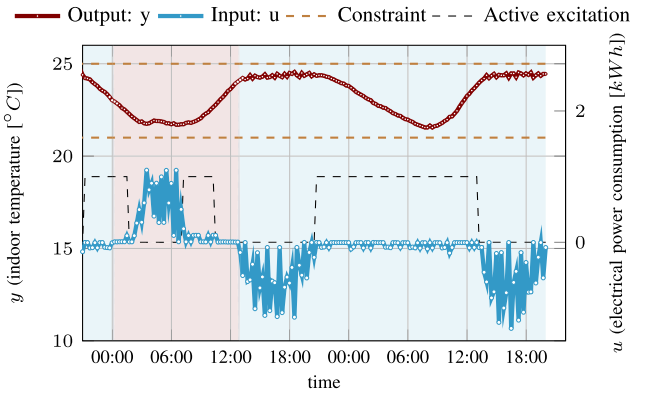


Fig. 7. Second experiment in Polydome: two-day running by the proposed robust data-driven control. The black line indicates the time interval within which the active excitation is active: high level: active and low level: inactive.

To better distinguish the heating and cooling modes in our plots, we use a positive input value for the heating mode and a negative input for the cooling mode. We further enforce the following input constraint to model the maximal energy consumption of the heating/cooling:

$$\begin{cases} 0 \text{ kWh} \leq u_i \leq 1.5 \text{ kWh}, & \text{heating mode} \\ -1.15 \text{ kWh} \leq u_i \leq 0 \text{ kWh}, & \text{cooling mode.} \end{cases}$$

Note that the HVAC unit consumes a constant 2.4 kWh of energy for ventilation, even without heating or cooling. The aforementioned input constraint excludes this basic ventilation power. The parameter \mathcal{E}_g in (10) is set by MATLAB command `DIAG(LINSPACE(0.2, 0.02, nc))`. The uncertainty set of the weather forecasts is estimated from an analysis of historical data as

$$\mathcal{W} := \left\{ w_i \left| \begin{bmatrix} -1^{\circ}\text{C} \\ -50 \text{ W/m}^2 \end{bmatrix} \leq w_i \leq \begin{bmatrix} 1^{\circ}\text{C} \\ 50 \text{ W/m}^2 \end{bmatrix} \right. \right\}. \quad (18)$$

B. Experimental Results

In this section, we describe four experiments that were conducted from May 2021 to June 2021. In particular, the first experiment shows the necessity of robust control, and the second experiment shows the adaptivity to mode switching. The third one runs a 20-day experiment to show the adaptivity and reliability of the proposed scheme, and the fourth one runs

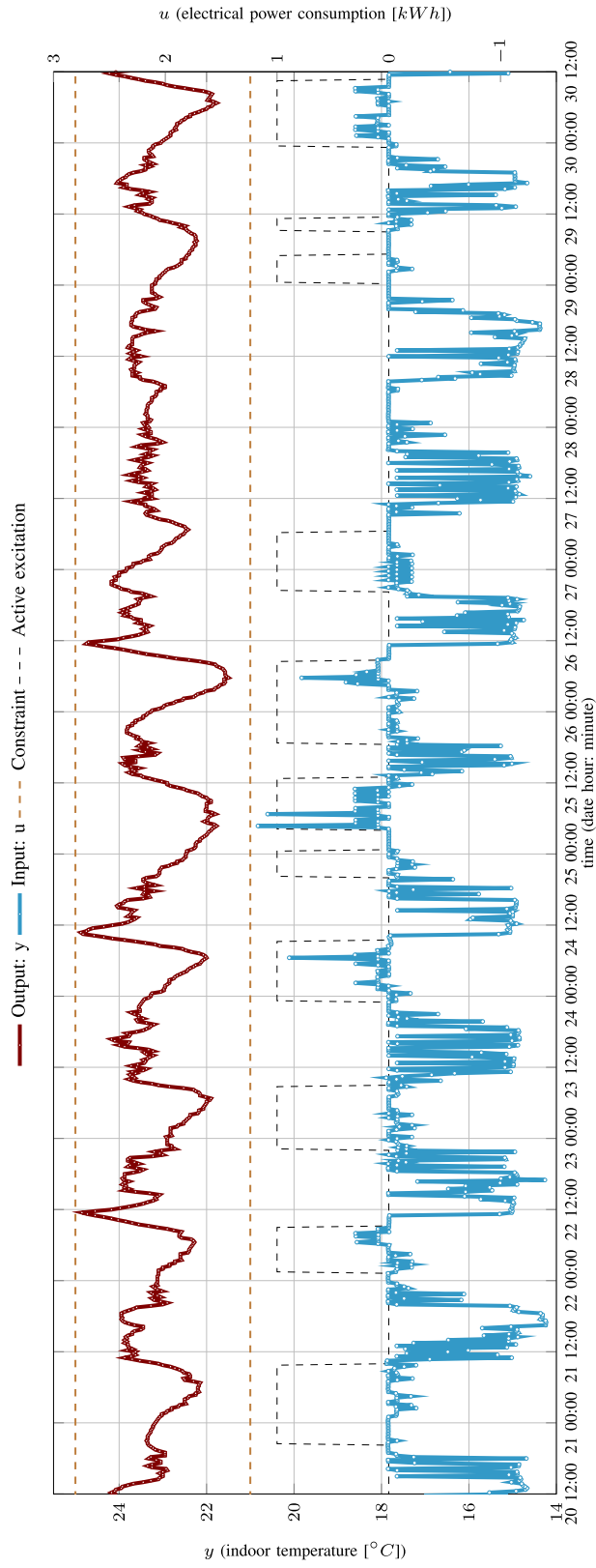


Fig. 8. Experimental results from noon 20th June 2021 to noon 30th June 2021: indoor temperature and electrical power consumption. The black line indicates the time interval within which the active excitation is active: high level: active and low level: inactive.

a four-day experiment to compare the proposed scheme with the default controller. Meanwhile, recall that we use a negative control input to represent cooling and a positive control input

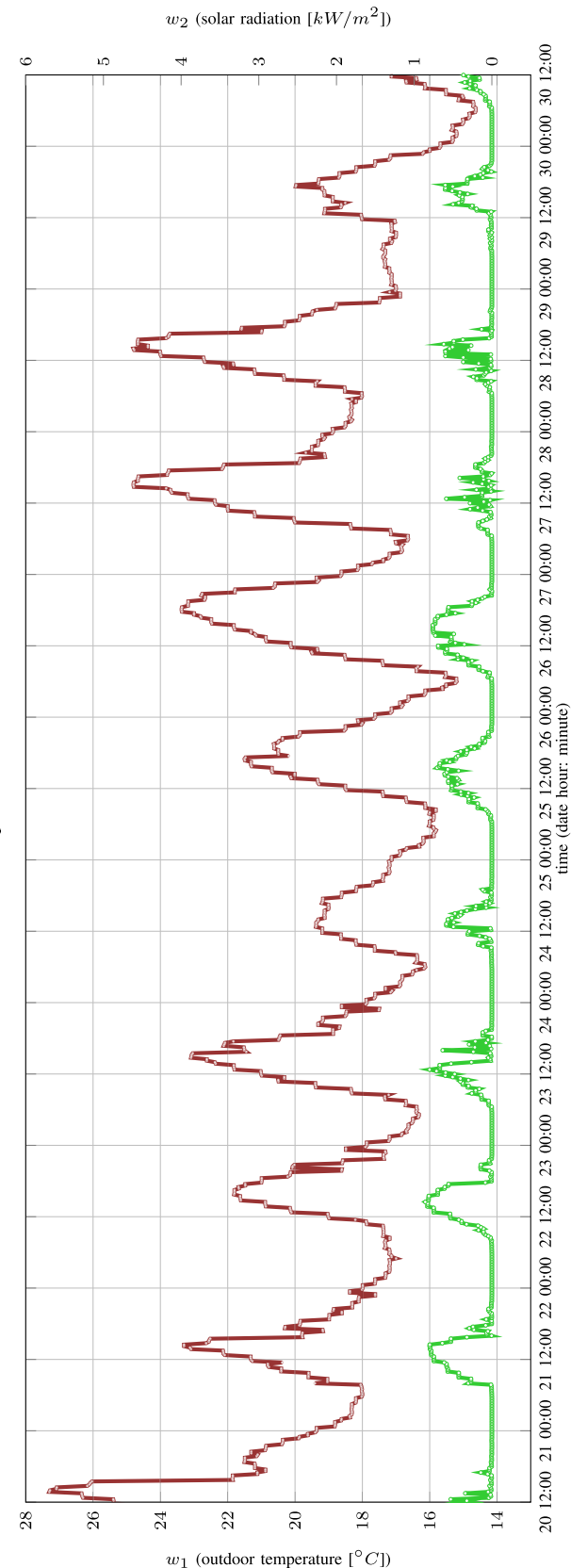


Fig. 9. Experimental results from noon 20th June 2021 to noon 30th June 2021: outdoor temperature and solar radiation.

for heating. Accordingly, we show the control input and system output (indoor temperature) within the same plot to better show the response from input to output.

1) *Experiment 1:* The first experiment includes two parts: a nonrobust version of the proposed scheme (i.e., $\mathcal{W} = \{\mathbf{0}\}$, $K = \mathbf{O}$) and a robust version with the uncertainty tube given in (18). In this test, we consider a time-varying indoor temperature constraint with respect to office hours, which is relaxed during the night and is tightened to ensure occupant comfort during office hours

$$\begin{cases} 21^\circ\text{C} \leq y_i \leq 26^\circ\text{C}, & \text{from 8 a.m. to 6 p.m.} \\ 19^\circ\text{C} \leq y_i \leq 30^\circ\text{C}, & \text{otherwise.} \end{cases}$$

The nonrobust experiment was conducted on May 14, 2021, and the result is plotted in Fig. 5. The HVAC system was in the heating mode throughout this experiment, and we can observe that the input was 0 until the indoor temperature hits the lower bound at around 4 A.M. Later, it started preheating the room to satisfy the office hours temperature constraint at around 6 A.M. However, we can still observe frequent but small constraint violations from 8 A.M. to 10 A.M., which then leads to overheating after 10 A.M.

In comparison, the robust controller effectively handled these issues in an experiment conducted on May 25, 2021. The result is shown in Fig. 6, where we used the same time-varying indoor temperature constraint. We can observe that the robust controller safely protects the system from violating the lower bound through the whole test, and it also successfully pre-heated the building to fit the time-varying indoor temperature constraint. The performance deterioration that occurred to the nonrobust controller after 10 A.M. was avoided as well, where the controller smoothly turned off the heating without unnecessary overheating.

2) *Experiment 2:* The second experiment is a pilot test to validate the adaptivity to the mode switching and the necessity of active excitation (see Algorithm 1). The experiment was conducted from May 28 to 29, 2021, with the result shown in Fig. 7, where the indoor temperature of this experiment is bounded within

$$21^\circ\text{C} \leq y_i \leq 25^\circ\text{C}.$$

This change of heating/cooling mode is depicted as a positive/negative control input and a red/blue shaded region in Fig. 7. However, it is noteworthy that the system was in the cooling mode on the second evening. If there was no active excitation, the cooling should be off through the night to minimize energy consumption, and the Hankel matrices used for the controller would have lost persistent excitation. Instead, the active excitation, which is depicted as small fluctuations from 0:00 to 8:00 on the second day, maintained the persistency of excitation. The excitation signal is randomly selected as follows:

$$\begin{cases} 0 \text{ kWh} \leq u_{e,i} \leq 0.1 \text{ kWh}, & \text{heating mode} \\ -0.075 \text{ kWh} \leq u_{e,i} \leq 0 \text{ kWh}, & \text{cooling mode.} \end{cases}$$

In conclusion, the controller successfully carried out the task of energy minimization in this experiment. In particular, when there is no need for heating/cooling, such as during the second evening, only active excitation took effect to maintain the persistency of excitation. The heating/cooling also takes

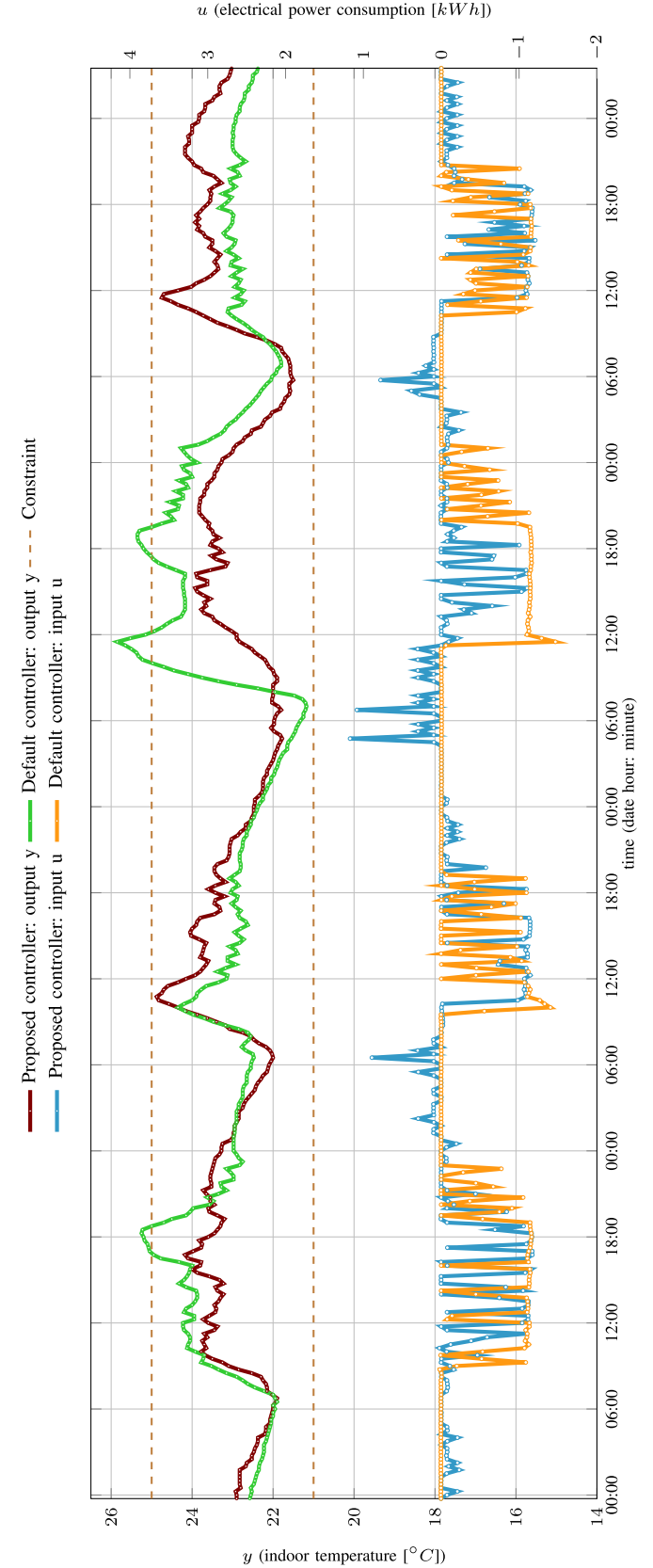


Fig. 10. Comparison of the proposed robust controller and default controller: indoor temperature and electrical power consumption.

effect to robustly maintain the indoor temperature within the constraints.

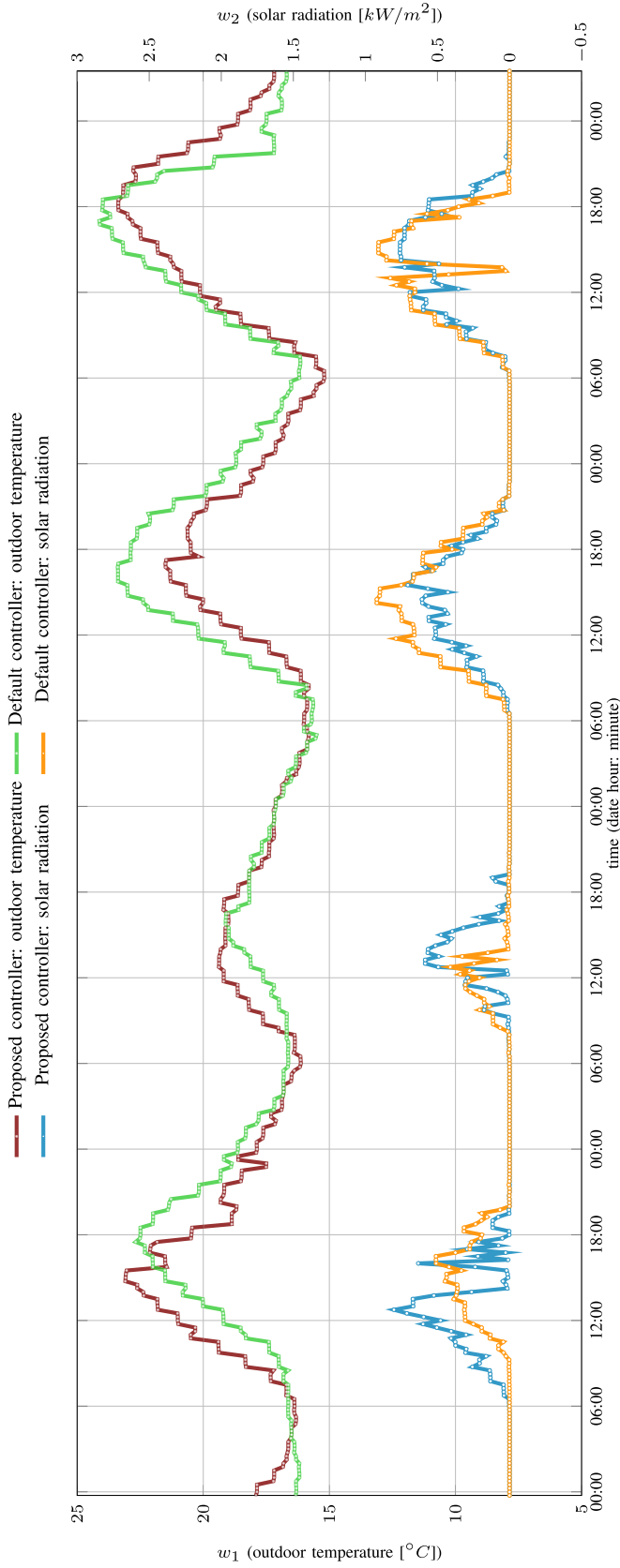


Fig. 11. Comparison of the proposed robust controller and default controller: outdoor temperature and solar radiation.

3) *Experiment 3:* This experiment was planned to validate the long-term reliability and adaptivity of the proposed controller. The experiment ran continuously for 20 days from June

TABLE III

STATISTICS OF THE 20-DAY EXPERIMENT				
average indoor temperature	average outdoor temperature	average solar radiation	duration of constraint violation	average hourly energy consumption
23.7°C	20.8°C	0.21W/m ²	0h	1.6kWh
min/max indoor temperature	min/max outdoor temperature	min/max solar radiation	hours of heating	hours of cooling
21.5°C 24.88°C	14.6°C 29.5°C	0W/m ² 0.89W/m ²	48h	432h

TABLE IV

STATISTICS OF THE FOUR-DAY COMPARISON

	average indoor temperature	average outdoor temperature	average solar radiation	duration of constraint violation
Proposed controller	23.1°C	18.5°C	0.17W/m ²	0h
Default controller	23.2°C	18.8°C	0.17W/m ²	5.75h
	min/max indoor temperature	min/max outdoor temperature	min/max solar radiation	averaged hourly energy consumption
Proposed controller	21.5°C 24.9°C	15.2°C 23.4°C	0W/m ² 0.80W/m ²	1.15kWh
Default controller	21.2°C 25.9°C	15.5°C 24.1°C	0W/m ² 0.92W/m ²	1.41kWh

10, 2021, to June 30, 2021. The statistics of this experiment is summarized in Table III, and we only plot results from the 20th 12:00 to the 30th 12:00 in Figs. 8 and 9 due to the space limit.⁷

Note that the weather varies a lot throughout this experiment, with the outdoor temperature even once surpassing 29 °C on the 20th and also once dropping below 15 °C on the 26th. Therefore, the experiment shows the adaptivity of the proposed controller to weather variation. Moreover, the cooling mode dominated the whole experiment, with only a few days of heating at night. The proposed controller gives a long-term guarantee of temperature constraint satisfaction (see Table III) while updating the Hankel matrices constantly. Regarding the data update, the active excitation scheme (see Algorithm 1) also occasionally took effect to ensure the persistency of excitation. The time intervals within which the active excitation are active are plotted by value 1 along the black dashed line in Fig. 8.

4) *Experiment 4:* Finally, we compare the proposed robust DeePC scheme with the default controller (see Section VI-A), which regulates the supply air temperature based on the return air temperature. A fixed setpoint at 22 °C is given to the default controller in order to ensure the occupants' comfort throughout the day. It is worth noting that the default controller is a benchmark controller widely used in the building control community [5], [31], [61].

The experiment with the proposed controller was conducted from July 23, 2021, to July 26, 2021, and the one with the default controller ran from July 7, 2021, to July 10, 2021. The indoor temperature and electrical power consumption are plotted in Fig. 10, alongside the statistics of these two experiments

⁷Full plots of the 20-day experiment are available on GitHub: https://github.com/YingZhaoeo/Building_results

summarized in Table IV. To ensure a fair comparison, the weather conditions for these two experiments were similar, as shown in Fig. 11.

From Table IV and Fig. 10, more constraint violation is observed from the default controller than the proposed controller. One major underlying reason is that the default controller runs without the knowledge of a weather forecast and only cooled down the building when the return air temperature reached 23 °C. We believe that this is the reason accounting for the constraint violation in the day-1 experiment of the default controller. If the default controller could have predicted high solar radiation and turned the cooling on constantly, the temperature constraint violation should have been avoided.

Besides the benefit of robust constraint satisfaction, the proposed controller is also more power efficient than the default controller under similar weather conditions, which, in particular, consumed 18.4% less electricity than the default controller (see Table IV). Note that, to maintain the data quality, the proposed controller ran the active excitation scheme (see Algorithm 1) regularly from 00:00 to 9:00. Thus, there is still the possibility to further improve the energy efficiency of the proposed controller.

VII. CONCLUSION

In this work, we propose a robust bilevel data-driven adaptive-predictive building controller based on Willems' fundamental lemma. The proposed scheme performs comparably to a classical model-based approach in a numerical simulation. The practical viability is shown by deploying the proposed scheme to a conference building on the EPFL campus, where, without extra modeling effort, our proposed scheme improves 18% energy efficiency and robustly ensures occupant comfort.

ACKNOWLEDGMENT

Yingzhao Lian is responsible for the framework of this work. Jicheng Shi is responsible for the experiment.

REFERENCES

- [1] *EMU Electronics AG*. Accessed: Jun. 1, 2021. [Online]. Available: <https://www.emuag.ch/>
- [2] *InfluxDB*. Accessed: Jun. 1, 2021. [Online]. Available: <https://www.influxdata.com>
- [3] *Tomorrow.io*. Accessed: Jun. 1, 2021. [Online]. Available: <https://www.tomorrow.io>
- [4] Z. Afroz, G. M. Shafiullah, T. Urmee, and G. Higgins, "Modeling techniques used in building HVAC control systems: A review," *Renew. Sustain. Energy Rev.*, vol. 83, pp. 64–84, Mar. 2018.
- [5] A. Aswani, N. Master, J. Taneja, D. Culler, and C. Tomlin, "Reducing transient and steady state electricity consumption in HVAC using learning-based model-predictive control," *Proc. IEEE*, vol. 100, no. 1, pp. 240–253, Jan. 2012.
- [6] F. Belić, D. Slišković, and Ž. Hocenski, "Detailed thermodynamic modeling of multi-zone buildings with resistive-capacitive method," *Energies*, vol. 14, no. 21, p. 7051, Oct. 2021.
- [7] A. Ben-Tal, L. E. Ghaoui, and A. Nemirovski, *Robust Optimization*. Princeton, NJ, USA: Princeton Univ. Press, 2009.
- [8] J. Berberich and F. Allgower, "A trajectory-based framework for data-driven system analysis and control," in *Proc. Eur. Control Conf. (ECC)*, May 2020, pp. 1365–1370.
- [9] J. Berberich, A. Koch, C. W. Scherer, and F. Allgower, "Robust data-driven state-feedback design," in *Proc. Amer. Control Conf. (ACC)*, Jul. 2020, pp. 1532–1538.
- [10] J. Berberich, J. Kohler, M. A. Müller, and F. Allgower, "Robust constraint satisfaction in data-driven MPC," in *Proc. 59th IEEE Conf. Decis. Control (CDC)*, Dec. 2020, pp. 1260–1267.
- [11] J. Berberich, J. Köhler, M. A. Müller, and F. Allgöwer, "Data-driven model predictive control: Closed-loop guarantees and experimental results," *Automatisierungstechnik*, vol. 69, no. 7, pp. 608–618, Jul. 2021.
- [12] J. Berberich, J. Kohler, M. A. Müller, and F. Allgower, "Linear tracking MPC for nonlinear systems—Part II: The data-driven case," *IEEE Trans. Autom. Control*, vol. 67, no. 9, pp. 4406–4421, Sep. 2022.
- [13] A. Bisoffi, C. De Persis, and P. Tesi, "Data-based stabilization of unknown bilinear systems with guaranteed basin of attraction," *Syst. Control Lett.*, vol. 145, Nov. 2020, Art. no. 104788.
- [14] A. Boodi, K. Beddiar, M. Benamour, Y. Amrat, and M. Benbouzid, "Intelligent systems for building energy and occupant comfort optimization: A state of the art review and recommendations," *Energies*, vol. 11, no. 10, p. 2604, Sep. 2018.
- [15] S. Boyd and L. Vandenberghe, *Convex Optimization*. Cambridge, U.K.: Cambridge Univ. Press, 2004.
- [16] D. A. Bristow, M. Tharayil, and A. G. Alleyne, "A survey of iterative learning control," *IEEE Control Syst. Mag.*, vol. 26, no. 3, pp. 96–114, Jun. 2006.
- [17] G. Ceusters et al., "Model-predictive control and reinforcement learning in multi-energy system case studies," *Appl. Energy*, vol. 303, Dec. 2021, Art. no. 117634.
- [18] G. T. Costanzo, S. Iacovella, F. Ruelens, T. Leurs, and B. J. Claessens, "Experimental analysis of data-driven control for a building heating system," *Sustain. Energy, Grids Netw.*, vol. 6, pp. 81–90, Jun. 2016.
- [19] J. Coulson, J. Lygeros, and F. Dorfler, "Data-enabled predictive control: In the shallows of the DeePC," in *Proc. 18th Eur. Control Conf. (ECC)*, Jun. 2019, pp. 307–312.
- [20] J. Coulson, J. Lygeros, and F. Dorfler, "Regularized and distributionally robust data-enabled predictive control," in *Proc. IEEE 58th Conf. Decis. Control (CDC)*, Dec. 2019, pp. 2696–2701.
- [21] J. Coulson, J. Lygeros, and F. Dorfler, "Distributionally robust chance constrained data-enabled predictive control," *IEEE Trans. Autom. Control*, vol. 67, no. 7, pp. 3289–3304, Jul. 2022.
- [22] C. De Persis and P. Tesi, "Formulas for data-driven control: Stabilization, optimality, and robustness," *IEEE Trans. Autom. Control*, vol. 65, no. 3, pp. 909–924, Mar. 2020.
- [23] S. Dempe, *Foundations of Bilevel Programming*. Cham, Switzerland: Springer, 2002.
- [24] F. Dörfler. (2019). *Data-Enabled Predictive Control of Autonomous Energy Systems*. Accessed: Nov. 5, 2021. [Online]. Available: http://people.ee.ethz.ch/~florian/docs/Slides/Dorfler_INI_2019.pdf
- [25] F. Dorfler, J. Coulson, and I. Markovsky, "Bridging direct and indirect data-driven control formulations via regularizations and relaxations," *IEEE Trans. Autom. Control*, vol. 68, no. 2, pp. 883–897, Feb. 2023.
- [26] D. Dowson and B. Landau, "The Fréchet distance between multivariate normal distributions," *J. Multivariate Anal.*, vol. 12, no. 3, pp. 450–455, 1982.
- [27] J. Drgoňa et al., "All you need to know about model predictive control for buildings," *Annu. Rev. Control*, vol. 50, pp. 190–232, Jan. 2020.
- [28] E. Elokdha, J. Coulson, P. N. Beuchat, J. Lygeros, and F. Dörfler, "Data-enabled predictive control for quadcopters," *Int. J. Robust Nonlinear Control*, vol. 31, no. 18, pp. 8916–8936, Dec. 2021.
- [29] M. K. S. Faradonbeh, A. Tewari, and G. Michailidis, "Input perturbations for adaptive control and learning," *Automatica*, vol. 117, Jul. 2020, Art. no. 108950.
- [30] W. Favoreel, B. D. Moor, and M. Gevers, "SPC: Subspace predictive control," *IFAC Proc. Volumes*, vol. 32, no. 2, pp. 4004–4009, Jul. 1999.
- [31] R. Godina, E. M. G. Rodrigues, E. Pouresmaeil, and J. P. S. Catalão, "Optimal residential model predictive control energy management performance with PV microgeneration," *Comput. Oper. Res.*, vol. 96, pp. 143–156, Aug. 2018.
- [32] L. Huang, J. Coulson, J. Lygeros, and F. Dorfler, "Decentralized data-enabled predictive control for power system oscillation damping," *IEEE Trans. Control Syst. Technol.*, vol. 30, no. 3, pp. 1065–1077, May 2022.
- [33] H. Kazmi, S. D'Oca, C. Delmastro, S. Lodeweyckx, and S. P. Corgnati, "Generalizable occupant-driven optimization model for domestic hot water production in NZEB," *Appl. Energy*, vol. 175, pp. 1–15, Aug. 2016.
- [34] Y. Lian and C. N. Jones, "From system level synthesis to robust closed-loop data-enabled predictive control," 2021, *arXiv:2102.06553*.

- [35] Y. Lian and C. N. Jones, "Nonlinear data-enabled prediction and control," in *Proc. 3rd Conf. Learn. Dyn. Control*, in Proceedings of Machine Learning Research, vol. 144, A. Jadbabaie et al., Eds. PMLR, Jun. 2021, pp. 523–534. [Online]. Available: <http://proceedings.mlr.press/v144/lian21a/lian21a.pdf>
- [36] J. Löfberg, "Minimax approaches to robust model predictive control," Dept. Elect. Eng., Linköping Univ., Linköping, Sweden, 2003, vol. 812. [Online]. Available: <http://www.control.isy.liu.se/research/reports/Ph.D.Thesis/PhD812.pdf>
- [37] J. Lofberg, "YALMIP: A toolbox for modeling and optimization in MATLAB," in *Proc. IEEE Int. Conf. Robot. Autom.*, Sep. 2004, pp. 284–289.
- [38] M. Maasoumy, B. Moridian, M. Razmara, M. Shahbakhti, and A. Sangiovanni-Vincentelli, "Online simultaneous state estimation and parameter adaptation for building predictive control," in *Proc. Dyn. Syst. Control Conf.*, vol. 56130, 2013, Art. no. V002T23A006.
- [39] G. Marafioti, R. R. Bitmead, and M. Hovd, "Persistently exciting model predictive control," *Int. J. Adapt. Control Signal Process.*, vol. 28, no. 6, pp. 536–552, Jun. 2014.
- [40] I. Markovsky and F. Dörfler, "Behavioral systems theory in data-driven analysis, signal processing, and control," *Annu. Rev. Control*, vol. 52, pp. 42–64, Jan. 2021.
- [41] I. Markovsky and P. Rapisarda, "On the linear quadratic data-driven control," in *Proc. Eur. Control Conf. (ECC)*, Jul. 2007, pp. 5313–5318.
- [42] I. Markovsky and P. Rapisarda, "Data-driven simulation and control," *Int. J. Control.*, vol. 81, no. 12, pp. 1946–1959, 2008.
- [43] M. Minakais, S. Mishra, and J. T. Wen, "Groundhog Day: Iterative learning for building temperature control," in *Proc. IEEE Int. Conf. Autom. Sci. Eng. (CASE)*, Aug. 2014, pp. 948–953.
- [44] E. Mocanu et al., "On-line building energy optimization using deep reinforcement learning," *IEEE Trans. Smart Grid*, vol. 10, no. 4, pp. 3698–3708, Jul. 2019.
- [45] H. Neudecker, "A matrix trace inequality," *J. Math. Anal. Appl.*, vol. 166, no. 1, pp. 302–303, May 1992.
- [46] J. Nocedal and S. Wright, *Numerical Optimization*. Cham, Switzerland: Springer, 2006.
- [47] J. G. Rueda-Escobedo and J. Schiffer, "Data-driven internal model control of second-order discrete Volterra systems," in *Proc. 59th IEEE Conf. Decis. Control (CDC)*, Dec. 2020, pp. 4572–4579.
- [48] F. Ruelens, B. J. Claessens, S. Quaiyum, B. De Schutter, R. Babuška, and R. Belmans, "Reinforcement learning applied to an electric water heater: From theory to practice," *IEEE Trans. Smart Grid*, vol. 9, no. 4, pp. 3792–3800, Jul. 2016.
- [49] P. Schmitz, T. Faulwasser, and K. Worthmann, "Willems' fundamental lemma for linear descriptor systems and its use for data-driven output-feedback MPC," *IEEE Control Syst. Lett.*, vol. 6, pp. 2443–2448, 2022.
- [50] G. W. Stewart, *Matrix Algorithms: Volume 1: Basic Decompositions*. Philadelphia, PA, USA: SIAM, 1998.
- [51] D. Sturzenegger, "Model predictive building climate control: Steps towards practice," Ph.D. thesis, Dept. Inf. Technol. Elect. Eng., ETH Zürich, Zürich, Switzerland, 2014. [Online]. Available: <https://research-collection.ethz.ch/handle/20.500.11850/98291>
- [52] R. S. Sutton and A. G. Barto, *Reinforcement Learning: An Introduction*. Cambridge, MA, USA: MIT Press, 2018.
- [53] A. Swales et al., "Open MODBUS/TCP specification," *Schneider Electr.*, vol. 29, pp. 3–19, Jan. 1999.
- [54] M. Tesfay, F. Alsaileem, P. Arunasalam, and A. Rao, "Adaptive-model predictive control of electronic expansion valves with adjustable setpoint for evaporator superheat minimization," *Building Environ.*, vol. 133, pp. 151–160, Apr. 2018.
- [55] H. J. van Waarde and M. K. Camlibel, "A matrix Finsler's lemma with applications to data-driven control," in *Proc. 60th IEEE Conf. Decis. Control (CDC)*, Dec. 2021, pp. 5777–5782.
- [56] J.-W. van Wingerden, S. Mulders, R. Dinkla, T. Oomen, and M. Verhaegen, "Data-enabled predictive control with instrumental variables: The direct equivalence with subspace predictive control," 2022, *arXiv:2209.05210*.
- [57] J. C. Willems and J. W. Polderman, *Introduction to Mathematical Systems Theory: A Behavioral Approach*. Cham, Switzerland: Springer, 1997.
- [58] J. C. Willems, P. Rapisarda, I. Markovsky, and B. L. M. De Moor, "A note on persistency of excitation," *Syst. Control Lett.*, vol. 54, no. 4, pp. 325–329, Apr. 2005.
- [59] L. Xu, M. S. Turan, B. Guo, and G. Ferrari-Trecate, "A data-driven convex programming approach to worst-case robust tracking controller design," 2021, *arXiv:2102.11918*.
- [60] X. Yan, Q. Ren, and Q. Meng, "Iterative learning control in large scale HVAC system," in *Proc. 8th World Congr. Intell. Control Autom.*, Jul. 2010, pp. 5063–5066.
- [61] S. Yang, M. P. Wan, W. Chen, B. F. Ng, and S. Dubey, "Model predictive control with adaptive machine-learning-based model for building energy efficiency and comfort optimization," *Appl. Energy*, vol. 271, Aug. 2020, Art. no. 115147.
- [62] Y. Yu, S. Talebi, H. J. van Waarde, U. Topcu, M. Mesbahi, and B. Acikmese, "On controllability and persistency of excitation in data-driven control: Extensions of Willems' fundamental lemma," in *Proc. 60th IEEE Conf. Decis. Control (CDC)*, Dec. 2021, pp. 6485–6490.
- [63] Z. Zhang and K. P. Lam, "Practical implementation and evaluation of deep reinforcement learning control for a radiant heating system," in *Proc. 5th Conf. Syst. Built Environ.*, Nov. 2018, pp. 148–157.